



The University of Texas at Dallas

AIAA DBF 2018-2019



1.0 Executive Summary.....
1.1 Mission Overview.....
1.2 Design Overview
1.3 Performance Capabilities
2.0 Management Summary
2.1 Team Organization
2.2 Milestone Chart
3.0 Conceptual Design
3.1 Mission Requirements
3.2 Design Requirements
3.3 Configuration Selection
3.4 Configuration Refinement
3.5 Final Conceptual Design
4.0 Preliminary Design
4.1 Design Methodology
4.2 Mission Model
4.3 Preliminary Sizing
4.3.1 Wingspan
4.3.2 Propulsion
4.4 Aerodynamics
4.4.1 Airfoil Selection
4.4.2 Drag Analysis
4.5 Stability and Control
4.5.1 Vertical/Horizontal Tail Sizing
4.5.2 Longitudinal Stability
4.6 Performance Estimates.....
5.0 Detail Design.....
5.1 Dimensional Parameters Table.....
5.2 Material Characteristics and Capabilities.....
5.2.1 Material Selection.....
5.3 Structural Design Selected.....
5.3.1 Fuselage.....
5.3.2 Wing and Tail.....
5.3.3 Propulsion.....
5.3.4 Controls and Servos.....
5.4 Sub-System Design and Integration.....
5.4.1 Electronics.....
5.4.2 Payload Mechanisms.....
5.4.3 Radome.....
5.4.4 Peripheral RF Actuation.....
5.5 Weight and Mass Balance.....
5.6 Flight and Mission Performance.....
5.7 Drawing Package.....
6.0 Manufacturing Plan.....
6.1 Manufacturing Methods Considered.....
6.1.1 Wing and Control Surfaces.....
6.1.2 Fuselage.....
6.1.3 Mechanisms.....
6.2 Manufacturing Methods Selected
6.2.1 Wing & Tail.....
6.2.2 Fuselage.....
6.2.3 Electronics Installation.....
6.2.4 Mechanisms Installation.....
6.3 Manufacturing Milestone.....
6.3.1 Manufacturing Schedule.....

7.0 Testing Plan.....
7.1 Test Objectives.....
7.2 Subsystem Testing.....
7.2.1 Propulsion Testing.....
7.2.2 RF testing.....
7.2.3 Aerodynamic Testing.....
7.2.4 Mechanism Testing.....
7.3 Flight Test Schedule and Flight Plan.....
7.4 Flight Checklists.....
7.4.1 Pre-Flight.....
7.4.2 Post-Flight.....
8.0 Performance Results
8.1 Demonstrated Performance of Key Subsystems.....
8.1.1 Propulsion Test Results.....
8.1.2 RF Test Results.....
8.1.3 Aerodynamic Test Results.....
8.1.4 Mechanism Test Results.....
8.1.5 Failsafe.....
8.2 Demonstrated Flight Performance of Completed Aircraft.....
Bibliography.....

Acronyms, Abbreviations, and Symbols

Description	Acronym
Unmanned Aerial Vehicle	UAV
Rotations Per Minute	RPM
Fastest Lap Time by any Team	$T_{min_overall}$
Fastest Lap Time by Individual Team	T_{min_team}
Nickel-Metal Hydride	NiMH
Ground Mission	GM
Computational Fluid Dynamics	CFD
Reynolds Number	Re
Angle of Attack (AoA)	α
Maximum Coefficient of Lift	Cl,max
Coefficient of Lift	Cl
Coefficient of Drag	Cd
Lift to Drag Ratio	L/D
Vertical Tail Area	Sv
Vertical Tail Volume Coefficient	Vv
Horizontal Tail Area	Sh
Horizontal Tail Volume Coefficient	VH
Vertical Tail Moment Arm	lv
Horizontal Tail Moment Arm	lh
Static Margin	SM
Center of Gravity	CG
Cruise Coefficient of Lift	Cl,cruise
Expanded Polypropylene	EPP
Cyanoacrylate	CA
Acrylonitrile Butadiene Styrene	ABS
Polylactic Acid	PLA
Electronic Speed Controller	ESC
Transceiver/Receiver System	TX/RX System
Battery Eliminator Circuit	BEC

1.0 Executive Summary

This report documents the design, fabrication, and testing of Enalp, the submission to the Design-Build Fly Competition by The University of Texas at Dallas. The objective of the 2018-2019 American Institute of Aeronautics and Astronautics (AIAA) Design Build Fly (DBF) competition was to design and fabricate a multi-purpose aircraft that would support carrier operations. The plane would have to pass 4 major competition requirements. The first of these requirements would test if the plane were to fit in a box with a cross section of 3 feet wide by 2 feet tall, modeling the stowed configuration of planes on aircraft carriers. The second requirement is the aircraft's ability to remotely change from a stowed to flight configuration. The aircraft will also be judged based on if it can take off from a 5-degree launch ramp with a runway length of 10 feet and a runway width of 4 feet. For launch, the aircraft must also have a tail hook attached to the end of the plane. In addition, the aircraft must have a rotating radome on top of the fuselage and, at the minimum, 4 attack stores situated on the wings. These attack stores have a 3-inch diameter and weigh an estimate of 2.2 oz.

1.1 Mission Requirements

The final competition would take place in Tucson, AZ and would be split up into 3 flight missions and 1 ground mission. Mission 1 (M1) showcases the planes ability to take off without a payload and perform 3 laps of the designated course within 5 minutes. During M1 the plane will be expected to begin from the stowed configuration and take off from the launch ramp. Mission 2 (M2) involves the spinning radome, attached to the top of the fuselage. During M2 the aircraft will be expected to perform 3 laps within 5 minutes. For the final mission, Mission 3 (M3), the plane would take off with attack stores and will be judged based off of how many successful payload release laps performed. For M3, the plane would fly within a 10-minute window. For all missions, the plane would fly at a height of 15 feet.

1.2 Design Overview

The design was chosen that would effectively accomplish the mission parameters was a single motor conventional wing. The wing would be constructed out of balsa, basswood,



Figure 1: Third Flight Test

and foam which all together would have to be strong enough to carry multiple attack stores. To increase the structural stability, a carbon fiber boom was used to decrease the torsional and shear stresses. A conventional tail was chosen as the horizontal stabilizer and would be constructed mainly out of foam to reduce overall weight. All electronics would be housed in the fuselage of the aircraft. The course was estimated to be 3000ft and includes two 180 degree turns and a full 360-degree loop. At the first turn, the aircraft would be expected to drop an attack store, constituting a successful payload release lap. To target 10 successful payload release laps, the aircraft would have to fly with an idealized wind speed 8.5 m/s.

1.3 Performance Capabilities

To accomplish our overall design goals, the aircraft had to accomplish the following parameters.

1. Launch off a 10 ft ramp at a 5-degree incline
2. Cruising speed of 8.5 m/s
3. Takeoff speed of 5 m/s
4. Able to drop 4 payloads during M3 remotely
5. Empty Weight of 1.14 kg
6. Total Weight of 2.32 kg
7. Able to remotely turn on and off an onboard radome

2.0 Management Summary

2.1 Team Organization

The 2018-2019 University of Texas at Dallas Design Build Fly team consists of fifteen students who are participating on a voluntary basis. The team is composed of three seniors, six juniors, four sophomores, and two freshmen. Leadership consists of a Team Manager, Chief Engineer, and 3 sub-team leads. This hierarchical structure of the team allows for responsibilities to be delegated among the three sub-teams and is showcased in Figure 2.

The overall team is administered by the Team Manager who serves as an advisor and oversees the design process. This member organizes meetings, updates members on logistical affairs, and manages the DBF budget. In addition to these tasks, the Team Manager handles sponsorships and the travel logistics needed to get the team to the competition. The Chief Engineer supervises the design & build process, provides technical support to the sub-teams and manages deadlines. The Chief Engineer's other responsibilities include creating an agenda for each meeting, determining deliverables for each sub-team, and finalizing components that must be ordered. The Team Manager and Chief Engineer work closely together to resolve any conflicting ideas that may arise throughout the design and build process.

The sub-teams are divided into Aerodynamics & Modeling, Fabrication & Materials, and Electronics & Propulsion. Each sub-team has a designated team leader, who acts as the point of contact. The sub-team leads are responsible for working with their team members to design their subsystem and communicate with other sub-teams to integrate their components into a complete aircraft. Weekly meetings begin by the sub-team leads updating the team on their progress and taking suggested changes into consideration. The teams then break off and continue working on their deliverables. Final design decisions are made by the Team Manager and Chief Engineer.

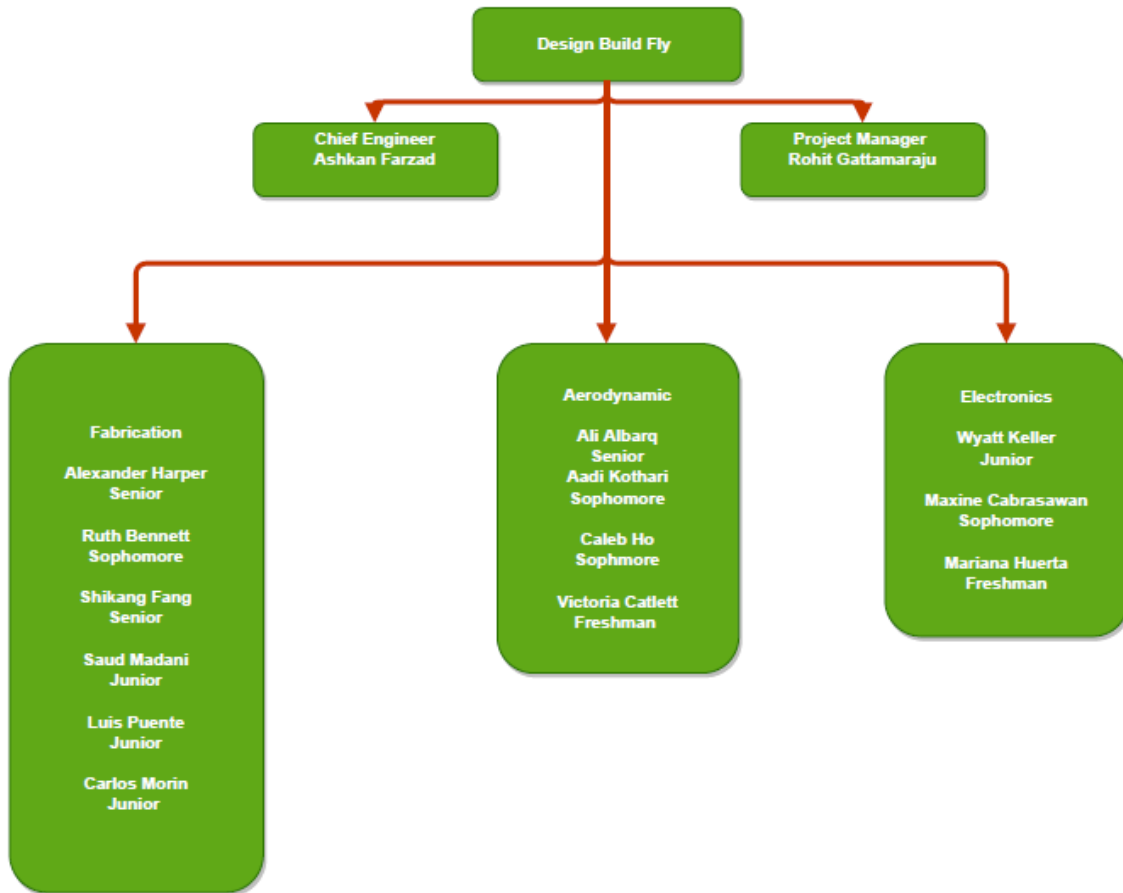


Figure 2: Management Flowchart

3.0 Conceptual Design

In order to determine a design that most accurately accomplishes the missions, a sensitivity study was conducted to see what affected the total score most. To do this, many different aircraft styles were considered and tested to maximize the total score.

3.1 Mission Requirements

The Design Build Fly competition for 2018-2019 simulates an aircraft carrier support plane. To mimic this type of aircraft, the plane is required to take off from a launch ramp, have a rotating radome, and carry attack stores. A requirement for all missions is to start in a stowed position and then lock into a flight configuration remotely. After locking into the flight configuration, the plane will be held using its tail hook and will be released upon reaching 70% of its maximum RPM. After release, it will have 10 feet to build up speed before reaching the end of the launch ramp. The plane will then follow a designated lap. Each lap will consist of two 1000 ft straightaways, two 180 degree turns, and a full 360 degree loop. The aircraft will take off against the wind and will land in the same direction. This is shown in Figure 3 as seen below.

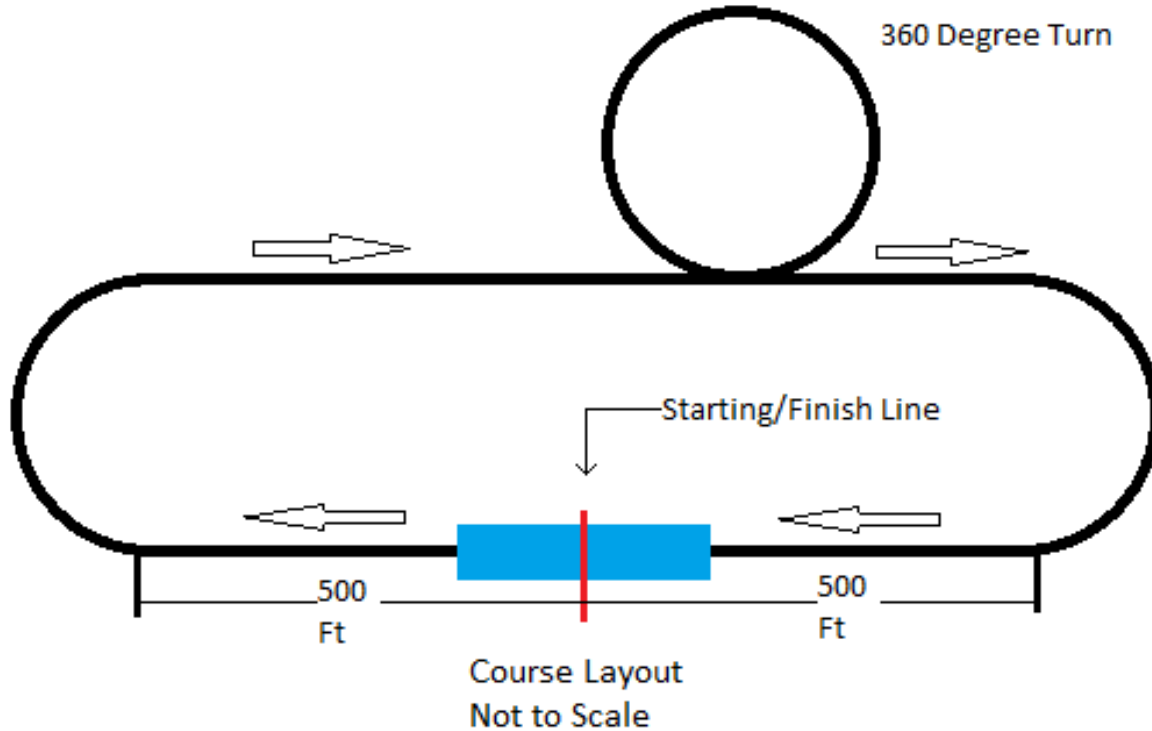


Figure 3: competition course laid out by AIAA

3.1.1 Scoring Summary

The final report score serves as a multiplier for the mission score to yield the final score, as given in the following equation:

$$\text{Total Score} = (\text{Report Score}) * (\text{Mission Score})$$

The total mission score is given as a sum of the three flight missions (M_1, M_2, M_3) and the ground mission (GM). Therefore, the equation of the total score becomes:

$$\text{Total Score} = (\text{Report Score}) * (M_1 + M_2 + M_3 + GM)$$

3.1.2 Mission Scoring

Mission 1: Delivery Mission

The aircraft must remotely enter the flight configuration from the stowed configuration in less than 5 minutes. Then, the aircraft must take off from the ramp, complete 3 laps in less than 5 minutes, and successfully land. For this mission, attack stores or a radome will not be added to the plane. To receive full points, the plane must land successfully.

M₁ Score: 1.0 points if the mission is completed successfully

Mission 2: Reconnaissance Mission

This mission is like *Mission 1* with the addition of a rotating radome. The crew will install the radome. Then, the aircraft must remotely enter flight configuration from the stowed configuration in less than 5 minutes. Then, the aircraft must take off from the ramp, complete 3 laps within 5 minutes, and successfully land. During each lap, the radome must be stationary until after the first 180-degree turn, then rotate until the final 180-degree turn.

M₂ Score: T_{min_overall} is the fastest lap by any team and T_{min_team} is the fastest lap by the individual team.

$$M_2 = 1 + T_{\min_overall}/T_{\min_team}$$

Mission 3: Attack Mission

Teams will attach their attack stores to the aircraft in the staging box. Then, like the other missions, the aircraft must remotely enter the flight configuration from the stowed configuration in less than 5 minutes. The aircraft will take off from the ramp and complete as many laps as possible in 10 minutes. A lap will count towards scoring if the aircraft drops exactly one attack store on the downwind leg of the lap. The score will only count if the aircraft lands successfully.

M₃ Score:

$$M_3 = 2 + (\text{number of scoring laps})$$

Ground Mission

For this mission, the plane, an uninstalled radome, and 4 attack stores will be in a “mission box”. The goal for the ground mission is for an assembly crew to show that each component can be successfully attached. The mission is then split up into two sub-missions, attaching the radome, and attaching the attack stores. Each submission will begin in the stowed configuration and time will start once the signal is given to the plane to lock into flight configuration. The radome must be shown to activate remotely and

each of the payloads must be shown to drop separately. Upon completion, the subassemblies must be taken off the plane. Scoring for this mission relies on the minimum time for all teams.

Ground Mission Score:

$$GM = (\text{Minimum Time of all Teams} / \text{Time of current team})$$

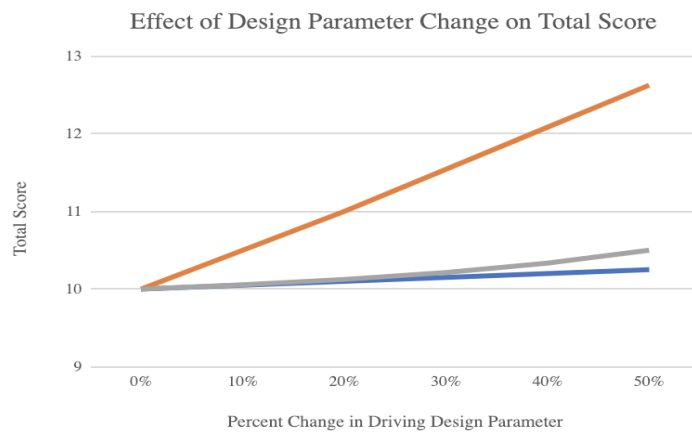
3.1.3 Score Sensitivity Analysis

In order to provide a constraint on the maximum score of *Mission 3*, we assumed an airspeed of 20 m/s. Given the approximate 3,000ft (914.4m) length of the track and 10-minute time frame, an aircraft could theoretically complete 13 scoring laps. However, given the short takeoff run, we will assume the maximum of 4 scoring laps.

Table 1: Mission Requirements

Mission #	Description	Score Equation	Objective	Design Parameter	Maximum Score
Mission 1	Complete 3 full laps in a 5 minute window	$M1 = 1.0$ (completed)	Complete three laps	N/A	1
Mission 2	Complete 3 full laps in a 5 minute window with the rotating radome attached	$M2 = 1 + \text{Min_time} / \text{N_time}$	Minimize lap time	Tlap	2
Mission 3	Drop exactly one store per lap to earn a point for that lap	$M3 = 2 + \#scoring_laps$	Maximize number of scores dropped , Minimize lap time	Tlap , Nstores	12
Ground Mission	Time trial to install radome, then replace radome and install four attack stores	$GM = \text{Min_time} / \text{N_time}$	Minimize replacement time	Trep	1

Table 2: Sensitivity Study



Clearly, changes in *Mission 3* have the largest effect on the overall score. Thus, we chose to focus on maximizing the number of attack stores that our aircraft could drop while remaining within design constraints.

3.1.4 Constraints

Battery: The battery was required to be Nickel Metal Hydride or a Nickel Cadmium. No Lithium batteries are allowed for the competition. This created a significant hurdle as it was hard to find a vendor that would provide a battery that would give the required voltage and capacity to sustain 10 minutes of flight time. Our team decided it would be best to create a NiMH battery using 36 cells. There was no maximum weight for batteries this year.

Launch Ramp: The plane would begin on the launch ramp at a 5° incline and be expected to take off before reaching the end. The dimensions of the ramp are 10 ft by 4 ft.

Stowed Configuration: The stowed configuration of the aircraft must fit within a 2 ft by 3 ft staging box. It must be capable of remotely transitioning into the flight configuration.

Rotating Radome: The radome must be at least 12 inches in diameter and one inch thick in the center. It must be able to rotate on command and be clearly visible.

Attack Stores: The attack stores are dart rockets with a 3-inch diameter and a 10-inch length. The aircraft must carry a minimum of 4 attack stores, and each store must have a clearance of 0.5 inches from the aircraft (excluding the mounting mechanism) and other attack stores. Each store must be capable of being individually and remotely deployed.

Receiver: The aircraft receiver must have a “fail-safe” mode so that in the event of a signal loss, the aircraft will close the throttle, put the flaps down, put the elevator up, and put the ailerons and rudder in the full right position.

3.2 Design Requirements

Launch Ramp: Taking off in 10 ft while fully loaded was one of the hardest constraints to overcome. To achieve this goal, the plane must be designed for low speed/high lift situations. An optimal aspect ratio must be used in order to generate a large amount of lift during high angles of attack.

Radome: Attaching a spinning radome on the centerline of the aircraft posed its own unique set of challenges. The aircraft must be able to brave the extra drag generated, while supporting a spinning disk sitting 6 inches above the fuselage. This required the design to include a sturdy tail boom and a small vertical stabilizer to clear the radome.

Attack Stores: The attack stores severely penalized lift and drove down the effective span of the wing. This translates to less lift being generated over all and hurting the takeoff performance of the aircraft. A longer wingspan is needed to compensate for the loss in lift and the weight of the aircraft must be minimized to assure a 10 ft takeoff capability.

3.3 Configuration Selection

Several different configurations were brainstormed throughout the design process. One of the first ideas considered was the conventional folding wing up/down in order to meet the size constraint. This idea was dismissed because it interfered with the plane's height constraint. Due to larger wingspans, necessary to generate enough lift for takeoff, the overall height in the folded down/up configuration would exceed the limitations from the constraints of the competition.

The second idea to be considered was a rotating wing. This concept drew inspiration from the Boeing V-22 Osprey [1] and would rotate the wing over the fuselage. This method allows for simple mechanisms to be used, however the long wingspan would extend past the motor. This scenario would violate the 2 ft depth constraint, causing other ideas to be pursued.

The third idea considered was the idea of telescoping the wing in order to decrease the wingspan to meet the size requirement. This idea met difficulty in preserving the inner structure when in flight. The space for the inner ribbing would be taken up by the space used for housing the wing when in the stowed configuration. Thus, the idea was deemed implausible.

The design that was settled upon was the folded back wings configuration. These wings gave the possibility of an unlimited wingspan. Given this, we considered the two possibilities of putting the hinge at the front or hinge at the back of the wing. However, having the wings hinge at the front would cause the wings to overlap or run into each other when we tried to keep it within the regulations. So it was decided to have the wings hinge at the back. When retracted, the wings were not overlapping given the correct restraints and kept us within the competition's regulations. Further detail can be found in sections Mechanisms Installation (6.2.4) and Testing Mechanism (8.1.4).

Once the folding mechanism aspect was decided, it was determined that this configuration would best compliment a single engine, single winged aircraft. The decision matrix used to select these parameters is shown below in Table#. Configurations that were deemed inefficient received a score of 1, which is the lowest possible score. On the contrary, the more feasible ideas received a score of 5 and the totals were added up. The ideas with the highest total score were selected to continue with. Additionally, due to the

mission requiring the dropping of payloads quickly, the aircraft was designed for optimal stability, mimicking the proportions of a Cessna 172.

Table 3: This table outlines the decision matrix that was used to determine aircraft configurations.

	Cost	Size Constraint	Manufacturing Difficulty	Durability	Effectiveness To Missions	Total
1 - 5; 1 = Lowest Score, 5 = Highest Score						
Bi-plane	1	2	1	1	3	8
mono-plane	3	3	3	2	2	13
Dual-motor	2	2	1	4	5	14
Single-motor	4	5	3	5	2	19
Tail-dragger	4	1	4	4	4	17
Traditional landing Config.	5	5	3	4	2	19

3.4 Configuration Refinement

The wing was chosen for optimal speed and stability utilizing the S1223 airfoil. The control surfaces were chosen to be minimal in order to increase the stability. The tail and wing were also made as large as possible in order to maximize lift for a short take off distance. The tail was chosen to compliment the wing airfoil and match the proven stable proportions of a Cessna. The folding wing mechanism could not support anything more than a single motor and rotating a biplane would have increased the complexity disproportionately to the gains.

The payloads will be attached utilizing a claw mechanism as seen in section 6.1.3. The claws will secure and release the payloads remotely after being clasped in place. The radome will be screwed on using an adaptor to attach it to the boom of the fuselage.

The folding wing mechanism was determined to require a high strength, but proved the most simple and easy to manufacture/repair as well as physically feasible option configuration, thus driving the following configuration considerations such as single motor and single wing

The folding wing mechanism was required to have high strength, but was the most simple to manufacture and repair while still being a feasible option. Other configuration decisions such as having a single motor and single wing were determined by the selection of the folding wing configuration.

3.5 Final Conceptual Design

The final conceptual design of the aircraft uses a 6 ft wingspan and a conventional tail design. The aircraft is equipped with ailerons, elevators, and rudder in order to maximize maneuverability and minimize

turning radius. With its current configuration, the aircraft will carry 4 attack stores and a radome between the wing and tailplane.

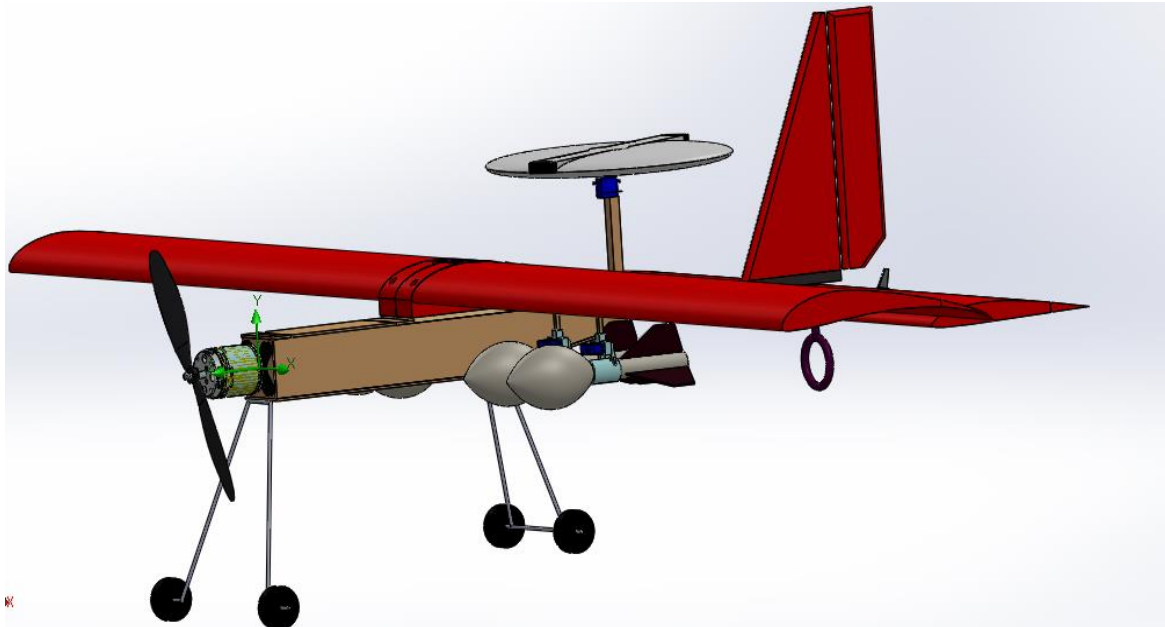


Figure 4: This is a model of the final conceptual design.

4.0 Preliminary Design

The preliminary design phase of the project was used to explore several different ideas and to optimize the parameters that would yield the highest final score possible. By taking into consideration the results of the score analysis, prototype optimization, and repetitive flights, the team selected the optimal parameters.

4.1 Design Methodology

The score analysis that was conducted gave the team a clear picture of which aircraft characteristics to focus on. The analysis proved that the most points are derived from deploying attack stores, therefore the main focus of the aircraft was to carry as much weight as fast as possible. An inherently stable and simple design was needed in order for the team to experiment with different methods of attaching the most amount of attack stores and the best way to convert into a stowed configuration. Common design elements were found among several real world aircraft that displayed the same flight characteristics the team sought after. Some of these design elements include: a high mounted wing, specific length ratios, and a range of stable static margin values. A second design consideration was to create a modular fuselage. This design would allow for timely repairs due to easy access to electronics, the engine, and wing mounts.

4.2 Mission Model

The flight course of the aircraft was broken into five distinct sections. This action was taken in order to determine potential problem areas that will need to be focused on more. The five sections of each flight are listed below:

- Takeoff: Takeoff is one of the major focuses of the aircraft. The aircraft must be capable of taking off in 10 feet while fully loaded.
- Climb: Climb was considered negligible due to aircraft performance during flight tests. The aircraft is predicted to climb to an altitude of 50 feet in Tucson, Arizona.
- Cruising: In this portion of the flight, the aircraft's lift is equal to its weight, and its thrust is equal to drag. This flight condition is designed to endure a maximum of 21 mph gusts of headwind.
- Turning: The aircraft is expected to make two 180 degree turns and one 360 degree turn. With this in mind, the aspect ratio of the wing was selected in a way to allow for a small turn radius and minimize altitude loss.

Some of the uncertainties surrounding the predicted flight characteristics include: different altitude, air temperature, and wind patterns. These uncertainties have been accounted for in the design of the aircraft by making certain the aircraft will be able to handle the worst conditions it could encounter.

4.3 Trade-Offs

The idea behind the design was to minimize wingspan and therefore simplify the mechanism needed to put the plane into its stowed configuration. As a result, the overall size and weight of all components were reduced.

4.3.1 Wingspan

The team took into consideration the importance of a well designed wing, and created a list of constraints that needed to be accommodated. Priority was given to takeoff performance and ensuring the plane can takeoff in 10 feet. The minimum wingspan of 4 feet was considered but it was determined that it could not generate the needed lift when outfitted with the attack stores. The attack stores and fuselage reduce the effective span of the wing, therefore the geometric span of the wing was increased to 6 feet. The longer wing drastically increases the lift generated at lower speeds and allows the plane to lift off the takeoff ramp, fully loaded, with a slight margin for error.

Once the wingspan was decided upon, a full scale sketch of it was drawn in order to find optimal placement for servos and attack stores. The team made certain that the longer wing could withstand heavy loadings with a 15% safety factor.

4.3.2 Propulsion

Table 4: Motor Selection Matrix

Motor	KV rating	Weight (g)	Thrust (g)	Cost (\$)	Watts	Max Current (A)
Turnigy D3530/14	1100	73	1100	16.82	910	40
Turnigy G60	500	360	2600	59.75	715	65
Monster Power 15	950	170	1100	34.95	425	42

Based on this data, the team picked the Turnigy G60 500Kv motor for its high thrust ratings and affordability. The motor was rated online to output 2.6Kg of thrust with a 14.4V battery and 13x7 propeller. This is exactly what was needed based on the calculations. The kWh for this specific motor was also very low. This fell within our parameters, the motor has a high thrust, was very efficient, and was relatively light.

4.3.3 Battery

Table 5: Battery Selection Matrix

Battery	Voltage (V)	Capacity (mAh)	Weight (g)	Cost (\$)
Turnigy Rechargeable Ni-MH Sub C cell (12 count)	1.2	1500	303	\$38.64
Tenergy Ni-MH 12V Pack w/ Connectors	12	2000	277	\$24.99
Tenergy Rechargeable Ni-MH Pack	8.4	3800	442	\$29.99

The power train batteries chosen were 24 NiMH Turnigy Rechargeable 1500mAh cells, soldered together into two packs of 12 in series. This was done in order to have a versatile method of configuring and producing the amount of power necessary for the plane's drive train. The ideal batteries for the challenges presented are rechargeable, due to both cost and ease of use. Arranged in a 12s2p orientation for the first test, after further flight

tests it was determined that the batteries needed to supply the motor with more power. This configuration of 1500mAh batteries allows for a combined burst of 30C, Approximately 45A. However, while each NiMH battery provides 10C continuous, it does not provide the necessary voltage. Thus, the batteries must be wired 12 in series, and connected in parallel with each other to double the capacity and decrease the internal resistance losses of the batteries.

The receiver battery will consist of 5 NiMh cells to power all the servo actuations and RF system electronics. These batteries are commercial NiMh battery cells and can be installed into a generic battery holder to be easily taken out and recharged when needed.

4.3.4 Electronic Speed Controller

Table 6: ESC Selection Matrix

ESC	Max Burst Current(A)	Max Cruise Current (A)	Weight (g)	Cost (\$)	BEC
Hobby King 30 A	40	30	32	10.60	UBEC
Hobby King 40 A	60	40	36	19.89	SBEC
Hobbywing Skywalker 80 A	100	80	82	32.99	UBEC

Our ESC was chosen because it is rated at 40 amps, which is high enough to allow us to test different motor sizes and configurations.

As shown by Table #([3]) of our report, multiple ESCs were considered before deciding on the best one for our control system. The team found the Hobby King 2-6S 40A SBEC to be the best option for our system due to various factors: cruise current, burst current, and weight. Considering that between 23A and 37A of current were continuously drawn by the motor used at 100% throttle, the 80A ESC was found to be excessive. Conversely, the 30A ESC was found to be too limited considering the motor could reach a burst current higher than 30A. Therefore, the 40A ESC was selected to be most appropriate for the amperage needed. The weight of the 40A ESC, 36 g, also presented an advantage for its selection, especially compared to the 82g of the 80A ESC. It was a clear choice to select the Hobby King 2-6S 40A SBEC once all of the parameters were taken into consideration.

4.4 Aerodynamics

The aerodynamic configuration was designed and analyzed using XFLR5 and SolidWorks Flow Simulation. XFLR5 is a graphically-oriented analysis program operating on XFOIL's panel method airfoil

analysis capabilities. SolidWorks Flow Simulation is an intuitive Computational Fluid Dynamics(CFD) solution embedded within 3D CAD that enables users to quickly and easily simulate liquid through or around designs, which was used to support theoretical data acquired from XFLR5 for wing lift characteristics.

4.4.1 Airfoil Selection

Using XFLR5 numerous airfoils were analyzed for takeoff and cruise conditions at Reynolds number of ~230,000 - 410,000, respectively. Figure # shows the lift properties at critical angles of attack , take off , and the drag polar at cruise for the best-performing airfoils in the study:

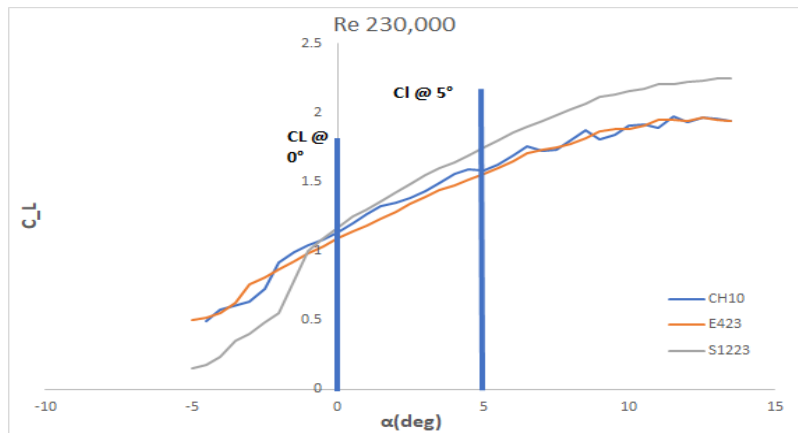


Figure 5: Coefficient of Lift Characteristics at Critical AoA (Take-off)

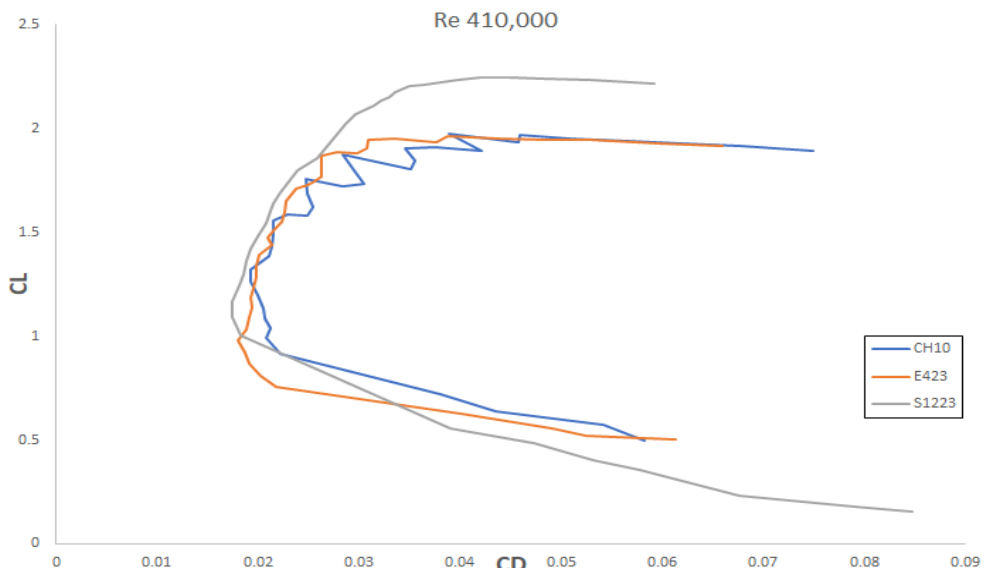


Figure 6: Cl vs Cd at Cruise Speed

Airfoils in this study were obtained from the University of Illinois-Urbana-Champaign Airfoil Database[2]. The S1223 airfoil was selected due to its high max coefficient of lift $C_{l,max} \sim 1.73$ at take off , better critical angle of attack (AoA) characteristics and most favorable angle of stall. As shown from the figures above, the CH10 airfoil has a better C_l at 0° than the E423 but lower than S1223 , higher C_l at 5° than E423 but still lower than S1223 , and results in a relatively high coefficient of drag C_d at cruising conditions, therefore it was deemed not efficient. The second airfoil is the E423, which has lower C_l at 0° and C_l at 5° than both S1223 and CH10 airfoils, and it showed most promising C_d at take off C_l , though , it was concluded that drag coefficient does not play a major role at takeoff as discussed in prior sections, so the E423 airfoil was also deemed inefficient. Since studies on these airfoils are done with low Reynolds numbers, the risk of stall is considerably high, so decision on the airfoil was based on the aforementioned characteristics relative to each other only. The team took in consideration that these value are a rough estimates to the airfoil characteristics due to XFLR5 software assuming idealistic values and in real world application, several factors can affect these results.

4.4.2 Drag Analysis

Considering the aircraft will undergo different missions, each mission configuration will have different components that will have different effects of drag. A breakdown of the main components drag coefficients are shown in the following table;

Table 7: Cd values of flight surfaces

Components	Cd
Wing	0.032
Vertical Tail	0.002
Horizontal Tail	0.008

From the table shown above, it is obvious that most of the drag comes from the wing and fuselage structure. For Mission 2, the aerodynamics team estimated a 20% increase in C_d caused by the surface area of the radome. For Mission 3, an estimated 13% increase in C_d caused by the surface area of the attack stores. The L/D ratio during the different missions was determined using XFLR5, shown in Figure #. The main takeaway from this study is that for Mission 2 & Mission 3, it is necessary for the aircraft to

operate as efficiently as possible to complete the missions fully. Since drag was over compensated in performance for Mission 2 & 3, it is assumed that there will be not any inefficiencies in Mission 1.

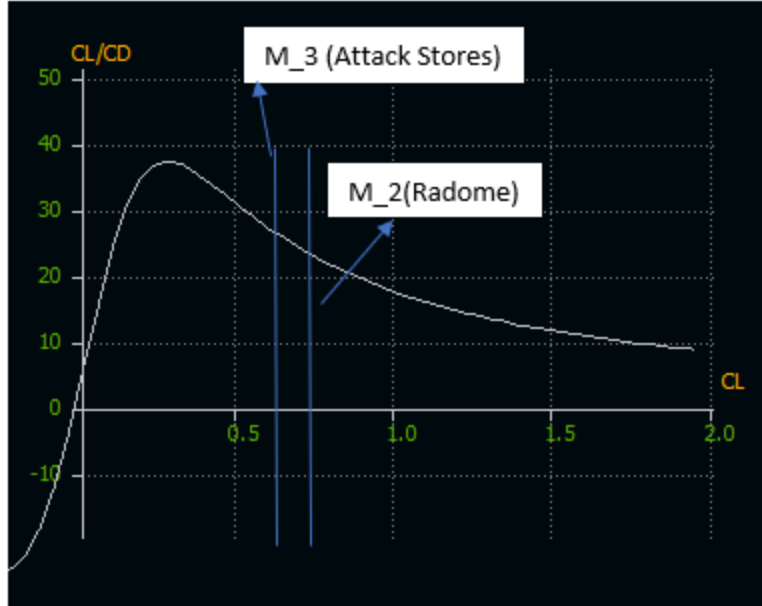


Figure 7: L/D Ratio During Different Mission Phases

4.5 Stability and Control

4.5.1 Vertical/Horizontal Tail Sizing

The main objective the chosen configuration is to determine an appropriate size for the vertical tail. Using the tail tail volume ratio relationship in Eq. # , the area of the vertical tail was determined.

$$V_v = \frac{S_v l_v}{S_b} \quad (\text{Eq } \#)$$

$$V_h = \frac{S_h l_h}{S_b} \quad (\text{Eq } \#)$$

The following vertical volume coefficient relationship was used to solve for the vertical tail area S_v with a volume ratio V_v of 0.04 that was based off a real scale of the Cessna 172, yielding a tail area of 20.3 square inches. However, it was discovered through flight test data, that the area found does not provide an efficient amount of yaw stability for a safe flight. This is believed to be inaccurate due to adapting volume ratio coefficient from a lifesize scale airplane. Through a few iterations, the optimal area for the vertical tail was decided to be 77.5 square inches. An added advantage to a larger tail provides the pilot with a better visibility at a greater distance. The dimensions of the vertical tail are as follows.

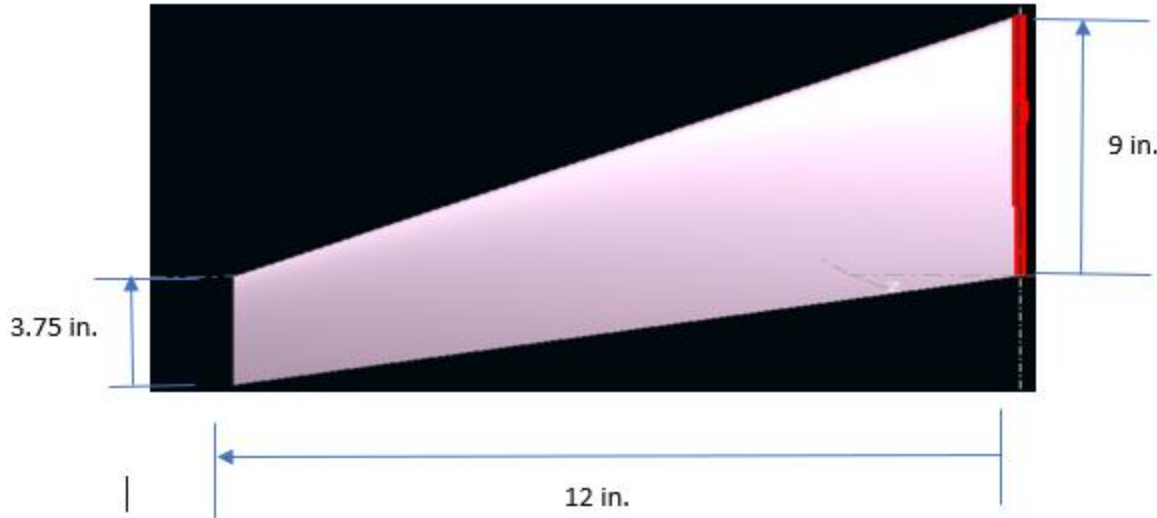


Figure 8: Vertical Tail Dimensions

Next, the appropriate size for the horizontal stabilizer is to be determined. Using the horizontal volume coefficient relationship in Eq. #, the area of the horizontal stabilizer S_h is found using the V_h to .6 which again corresponds to a life scale of Cessna 172. By maintaining an aspect ratio of a horizontal tail to be two-thirds the wing aspect ratio; $AR_h = \frac{2}{3} AR_w$, the area for the stabilizer is then calculated to be 325 inches squared, then through test data, a combination of different chord to length of the tail were iterated until the pilot was satisfied with the stability and behavior of the airplane in air. The dimension of the tail are as follows;

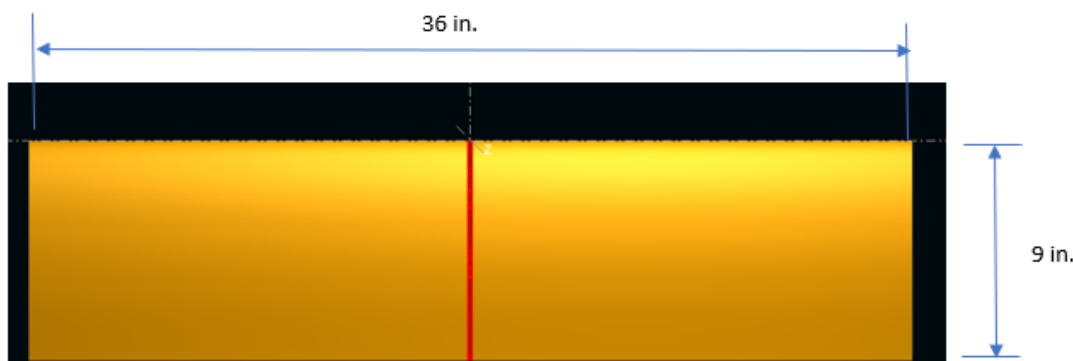


Figure 9: Horizontal Stabilizer

4.5.2 Longitudinal Stability

To ensure longitudinal stability, both XFLR5 and hand calculations were used and compared. Initially, the airplane was modeled into XFLR5 to observe the pitching moment C_M with the respect to the angle of attack. The results are shown in Figure # below;

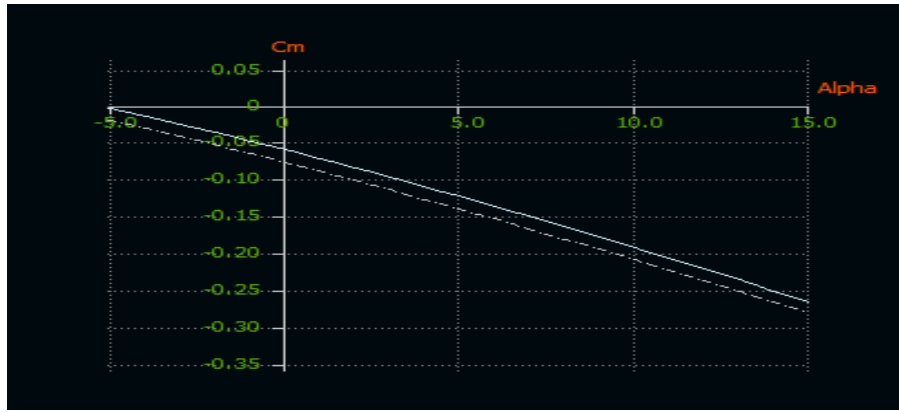


Figure 10: Default and elevator deflection of 5°(C_m) vs. α

The plot shows results for default configuration--wing tilt @ 4°--(solid) and an elevator deflection of 5° (dashed) to accommodate for take-off trim. The negative slope indicates the longitudinal stability. Additionally, the aircraft will trim at ~3°. After flight testing data, these plots agree with the aircraft's behavior. The equations describing both plots are as follows. Eq. 1 is for default configuration and Eq. 2 is for elevators deflected at 5°.

$$C_{M\alpha} = -0.0129\alpha - 0.0767 \quad \text{Eq. 1}$$

$$C_{M\alpha} = -0.0129\alpha - 0.0603 \quad \text{Eq. 2}$$

With pitching moment with respect to angle of attack $C_{M\alpha}$ of -.0129, it is determined that this aircraft will have positive longitudinal static stability, but only by a small margin. Static margin will therefore be $SM = .0129$. Preferably, a static margin of ~10-15% is recommended for most airplanes, and to achieve this, the Center of Gravity will be approximately 1.8 inches forward from the aerodynamics center. Since the aerodynamics center is located at almost 40% of the total chord of the design, the CG should be located at least 30% of the chord length. This will be approximately 3 inches away from the leading edge of the wing. Since the internal volume is limited in this design, placing the CG in the desired location is complex. To manage placing the CG where it is desired, the motor will be placed on balsa extended from leading edge of the fuselage. The batteries, electronics and other system components will be placed middle to forward of the fuselage. Weights could also be added to further improve location of CG, however, highly unrecommended because an unbalance of lift and weight may cause longitudinal stability to skew from stable.

4.6 Performance Estimates

As discussed earlier in section 3.1, Flight Missions 1 , 2 and 3 require that the aircraft must have the ability to fly a minimum of 3 laps within a 5 minute flying window. Mission 1 will not carry any payload,

while Mission 2 & 3 will carry payloads of a radome and attack stores, respectively. Detailed flight performance parameters are listed below in table 8.

Table 8: Performance parameters

Performance Parameter	M1	M2	M3
Cl max	1.833	1.833	1.833
Cl cruise	0.7	0.67	0.63
e	0.95	0.95	0.95
Cd	0.029	0.035	0.0328
L/D max	12	16	14
L/D cruise	25	27	29
Rate of Climb	6 ft/s	6 ft/s	6 ft/s
Vcruise	27.88 ft/s	31.68 ft/s	29.53 ft/s
Vstall	19.69 ft/s	22.96 ft/s	21.33 ft/s
Gross Weight	5.114 lb	5.16 lb	5.24 lb

4.6.2 Aircraft Component Analysis

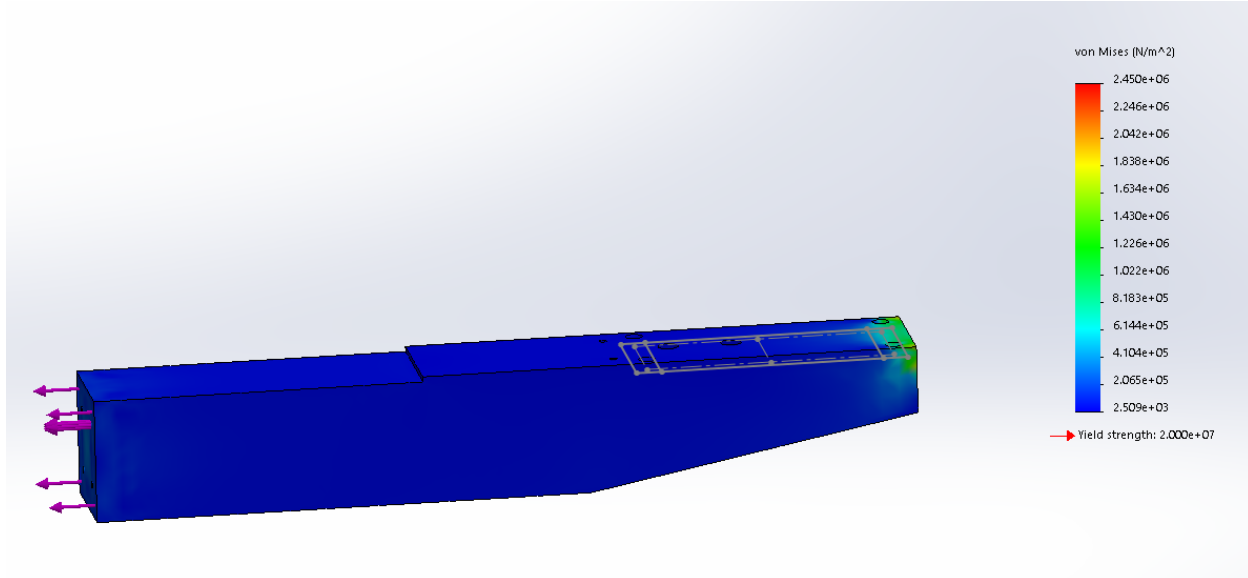


Figure 11: Take-off Stress Analysis For Tip of Fuselage

Figure 11 shown above was made to replicate the motor attached at the front at time of take off. This is to ensure that the motor will not rip off the fuselage upon attachment it on a tail hook. The results were conclusive of a sturdy structure of the fuselage, which will be used for the final aircraft.

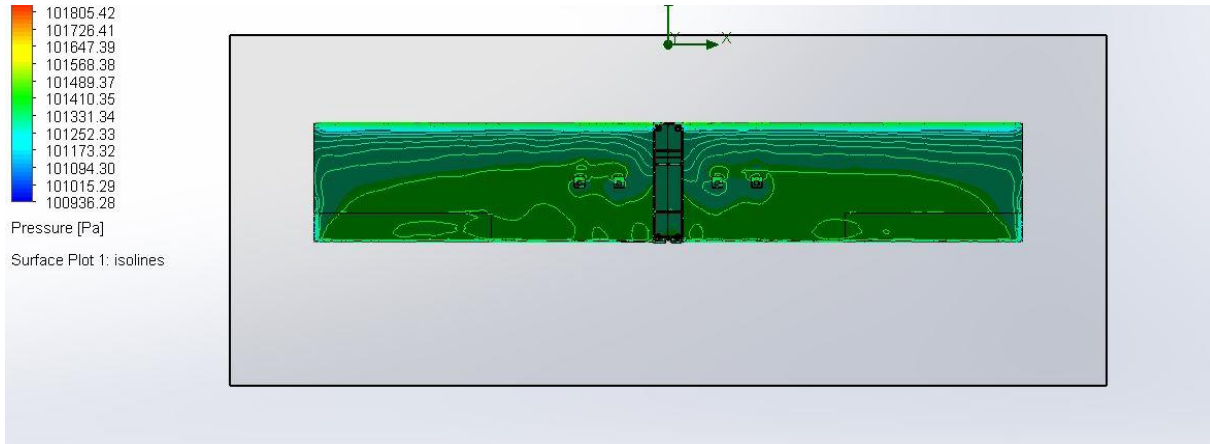


Figure 13: Isoline graph for pressure: Bottom view of the wing

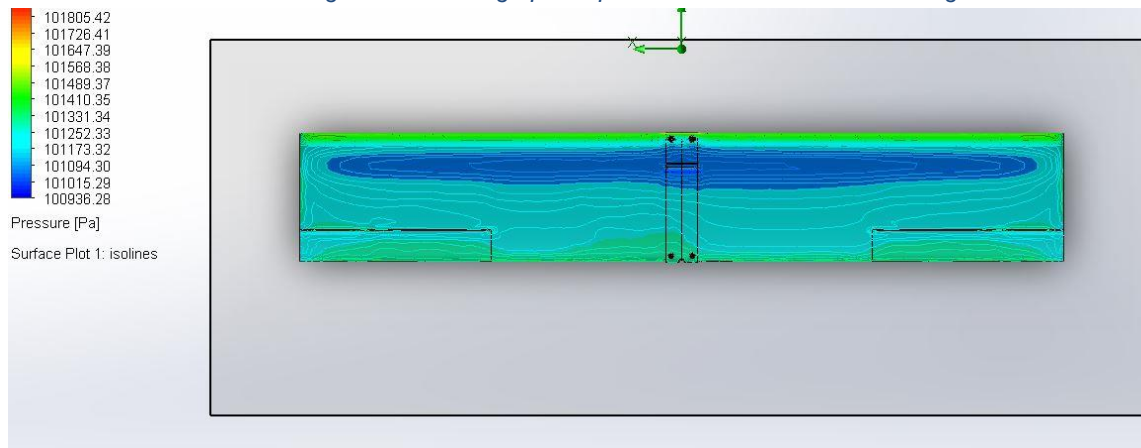


Figure 12: Isoline graph: Top view of the wing

The above isoline graphs shows more about the pressure distribution over the surface of a wing and also confirms its aerodynamic nature. There is a pressure gradient between the lower and upper surface of the wing, thus leading to an upward force of lift.

Table 9: SolidWorks Flow Simulation results.

Goal Name	Unit	Value	Averaged Value	Minimum Value	Maximum Value	Progress [%]	Use In Convergence	Delta	Criteria
SG Force (Y) 1	[N]	85.873	86.104	84.848	88.299	100	Yes	0.944	0.967

The CAD model of the wing was run through a SolidWorks flow simulation and the data represented in table 9 was collected from the study. The average normal force value in the Y direction is 85.87 N which is equivalent to 8.76 kg of lift which is well over the weight of plane which is 2.38 kg (5.24 lbs). This simulation gives us a good idea of whether the airplane will be able to provide enough lift force to take off.

5.0 Detail Design

5.1 Dimensional Parameters Table

Final aircraft dimensions were chosen based on values determined in the preliminary design stage. The aircraft consists of 5 major components: fuselage, wing, propulsion system, empennage, control systems. Aircraft basic dimensions are shown in the following table;

Table 5.1.1

Empennage		Fuselage	
Vertical tail span (in.)	12	Overall Length (in.)	31.75
Vertical tail geometric chord (in.)	6.4	Box Length(in.)	12
Vertical tail taper ratio	2.4	Taper Length(in.)	8
Vertical tail area (in^2)	77.5	Boom Length (in.)	11.75
Wing		Control Surfaces	
Horizontal tail span (in)	36	Wing span (in.)	72
Horizontal tail chord (in)	9	Chord (in.)	12
Horizontal tail area (in^2)	324	Area (in.)	864
		Ailerons area(in^2)	54
		Elevator area(in^2)	78.12
		Rudder area(in^2)	24

5.2 Material Characteristics and Capabilities

The material is designed to handle lift and payloads with a safety factor of 2. The goal for the materials selection was to optimize the trade-off between weight and strength as well as ease of manufacture.

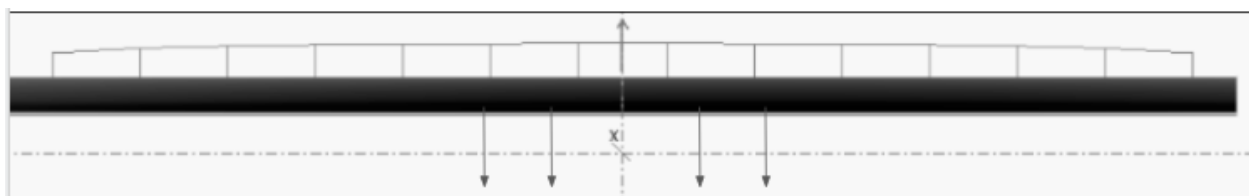


Figure 14: Lift distribution over wing.

Figure 14 shows the forces on the wing including the lift forces on the top and weight of payloads on the bottom.

5.2.1 Material Selection

Table 10: Properties of materials considered

	Considered Materials	Density (kg/m ³)	Tensile Strength (MPa)	Use on Final Plane
Wood	Balsa Wood	160	1.0	Ribs
	Basswood	450	2.4	Motor mount, spars
	Beech Wood	800	7	
Aerodynamic Covering	Canvas Fabric	1400	5520	
	Monokote	688	172	Cover Wings
Foam	Blue Core Foam	32	.065 ^[5]	
	Deprohn	36	.9	
	EPP Foam	110	1.1	
Adhesives	CA glue	1060 ^[6]	n/a	Wing Adhesive
	Duct Tape	920	20.7	Fuselage Reinforcement
	Epoxy	1100	n/a	Fuselage Adhesive
3D printed Material	Gorilla Glue	1138	n/a	
	ABS	1200	27	
	Carbon Fiber	1790	4413	Tail Boom
	PLA	1300	37	Mechanisms
	Steel	7870	440	Landing Gear, Control Rods

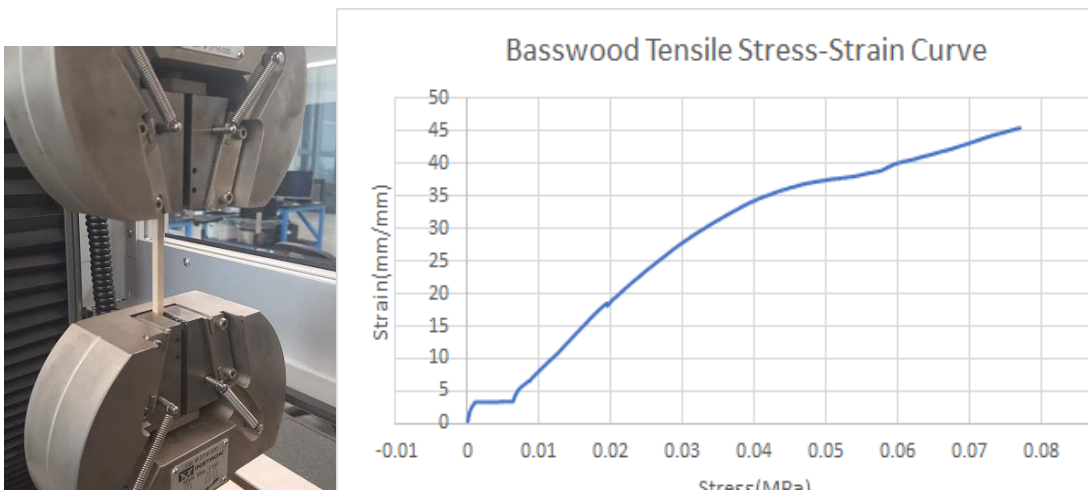


Figure 15: Basswood tensile testing.

Figure 15 shows the stress-strain curve of basswood as bought and used by the team being tested in a tensile test on an Instron Machine utilizing Bluehill software. This gives a more accurate sample of the wood being used in the plane and its material properties such as young's modulus and yield strength.

Frame:

Balsa wood was selected for the ribs with monokote wrapping to create the aerodynamic surface of the wings and tail in order to reduce weight while maintaining tensile strength throughout the wing. Basswood was selected for the spars and the motor mount for its density and strength at the cost of higher weight. The University of Texas at Dallas Materials Lab enabled a tensile test of one of the basswood spars allowing for more accurate analysis of the particular wood used in the plane(see figure 5.2.1.2). This compromise was necessary as these areas are exposed to greater stresses in flight, and the basswood presented a better alternative to the beech wood while still maintaining a factor of safety of 2 as seen in figure 5.2.1.1. Carbon fiber was selected for the tail boom in order to decrease the weight of the plane and to provide additional stability to the tail with the trade-off of the relatively high cost of the part. Steel was used for the control rods and landing gear legs due to its accessibility and it's reliable high strength and compressibility when very thin. The small size of the steel wire parts negated the high density of the material when it came to weight consideration. Epoxy was used to bond PLA and wood in the fuselage when attaching the various 3D printed parts, due to it's higher strength and better adhesive properties with plastics despite its longer cure time when compared to CA glue. Duct tape was used to reinforce the fuselage for simple repair and manufacture and to distribute the stress along the length of the body where it has greater tensile strength.

Other:

CA glue is used in the wings in order to ensure firm attachment of the spars to the ribs. CA glue provides almost instant strength which is very beneficial for expedient prototyping and manufacturing. Epoxy is used when bonding plastic to wood to ensure a solid, reliable connection. PLA is used for the 3D printed parts due to its accessibility and high tensile strength when machining precise parts.

5.3 Structural Design Selected

The team researched and experimented with many different structural designs and materials for the plane, including a solid foam wing, wooden rib wing with monokote wrapping, foam paneled fuselage, and balsa-paneled fuselage. The pros and cons of each design were researched and the methods of manufacturing were listed and compared. After a few iterations of prototyping and 3D simulations, it was decided that the wings would have a rib & spar structure made of balsa ribs and basswood spars, which would be wrapped with monokote to create the wing and tail surfaces. The fuselage was decided to have balsa exterior panels and basswood bulkheads.

5.3.1 Fuselage

The idea behind the structure of the fuselage is to minimize weight while keeping all the electrical components safely stored with the motor and wing fixed in their optimal positions. This required using balsa with the grain of the wood in the lengthwise direction (along with the length of the fuselage) on the side panels and cross-grained on the bottom and top. Additionally, multiple bulkheads throughout the fuselage, duct tape wrapping around the exterior of the fuselage, and the motor mount are implemented to keep the structure rigid with a minimal increase in weight.

A hollow rectangular carbon fiber tail boom was selected for the design to further decrease the weight of the plane while increasing the stability due to its large tensile strength to weight ratio.

5.3.2 Wing and Tail

The selected design for the wing and tail is with balsa ribs and basswood spars, which are wrapped with monokote to provide a smooth aerodynamic surface. The best rib profile was obtained using XFLR5 and double checked with SolidWorks Simulations. The wing and the tail are separated into five sub-assemblies, including the left wing, the right ring, the left tail, the right tail, and the vertical tail. The ribs are laser cut from $\frac{1}{8}$ inch balsa sheets to maximize accuracy. Three holes are cut out of the rib profile, one for running wire and the other two for saving weight. Ribs are spaced in a distribution mimicking the distribution of the loading due to lift on the wing. This distribution is roughly equal to \sqrt{x} with the largest

concentration located nearest the fuselage (see figure 16). There are two basswood spars that run the entire length of each wing and side of the horizontal tail. The spars are placed $\frac{1}{3}$ of the chord length from the leading edge of the wing. One is placed along the top edge and the other along the bottom for increased strength in the vertical direction to support the wing loading, as well as to offer easy replacement of ribs in the event of damage. The material of the spars was determined based on the amount of available space in the wing profile (figure 17) and tested in SolidWorks (figure 18), applying both the lift forces and force of weight on the spar and increasing the spar to ensure a safety factor of 2. The Vertical tail is formed of a flat piece of balsa to insure symmetry, ease of manufacture, and lightweight.

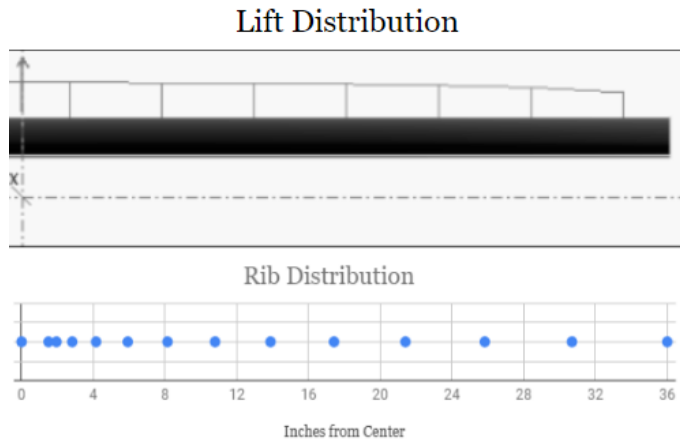


Figure 16: Lift distribution vs. spar locations

Tensile Strength of Square Material vs Thickness of Spar

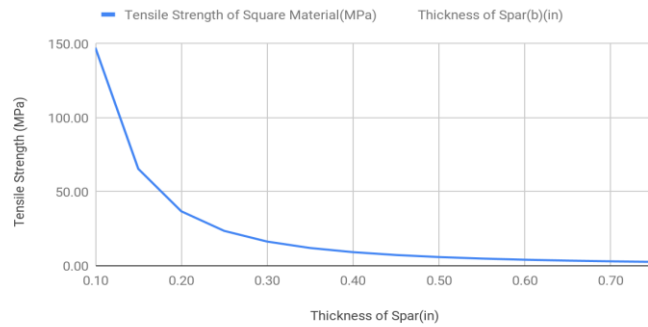


Figure 17: Tensile strength vs. thickness

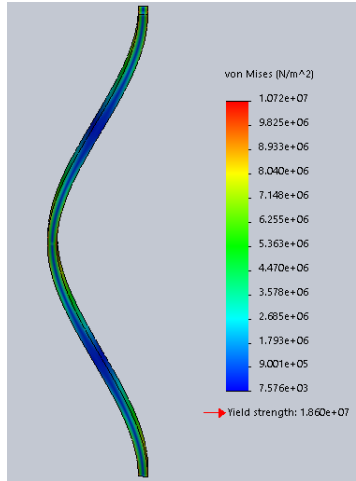


Figure 18: Simulation of weight and lift forces

The folding wing concentrates a lot of stress around the hinge of the mechanism so metal hinges were initially considered, however, their high density and high tolerances made them unsuitable. Instead, 3D printed PLA is used to form the hinges and a folding mechanism to take advantage of the ability to precisely manipulate the geometry and tolerances of the part. This allows for the creation of more effective and accurate parts saving on weight without sacrificing significant structural support. Similarly, the connection between the boom connection to the fuselage required unique and lightweight geometry and material due to the concentrated loading in that area. As for the horizontal tail to boom connection, a 3D printed PLA adaptor is attached with epoxy to the boom to keep it firmly in place. The horizontal tail spars are slid into slots in the sides of the adapter and secured with epoxy to the adapter. This allows the adapter to be fully customizable, easy to reproduce, and lightweight.

5.3.3 Motor Mount

The structure supporting the propulsion, bearing the thrust of the airplane, consists of one $\frac{1}{4}$ inch thick, square, basswood plate reinforced with two wooden beams and epoxy. This configuration is designed to minimize weight and reduce vibration and support the weight and force of the motor during flight, transferring its thrust force to the rest of the plane.

5.3.4 Controls and Servos

Servo motors with high rated stall torques and resilient gears are used to withstand the large loading against the ailerons and horizontal tail as they are moved to control the plane during flight. These servos are glued in place along the spars of the wings, spar rib structure and the tail boom with CA glue. The

control rods are made to be as short and taught as possible to limit the flutter of the control surfaces in flight and maximize their maneuverability. The control rods are affixed to the control surfaces with plastic control horns which are in turn attached to the surfaces with epoxy.

5.4 Sub-System Design and Integration

The electronics team and the fabrication collaborated closely on creating the sub-systems on the plane. The internal electronics and the exterior mechanisms are extremely important because they effects all the plane's functionalities and physical configuration. The following subsections gives a close look at these sub-system and integrations, including the electronics, payload mechanism, radome, peripheral RF actuation.

5.4.1 Electronics

To implement a functional electronic system we designed a wiring schematic showing the connections for all the electrical components:

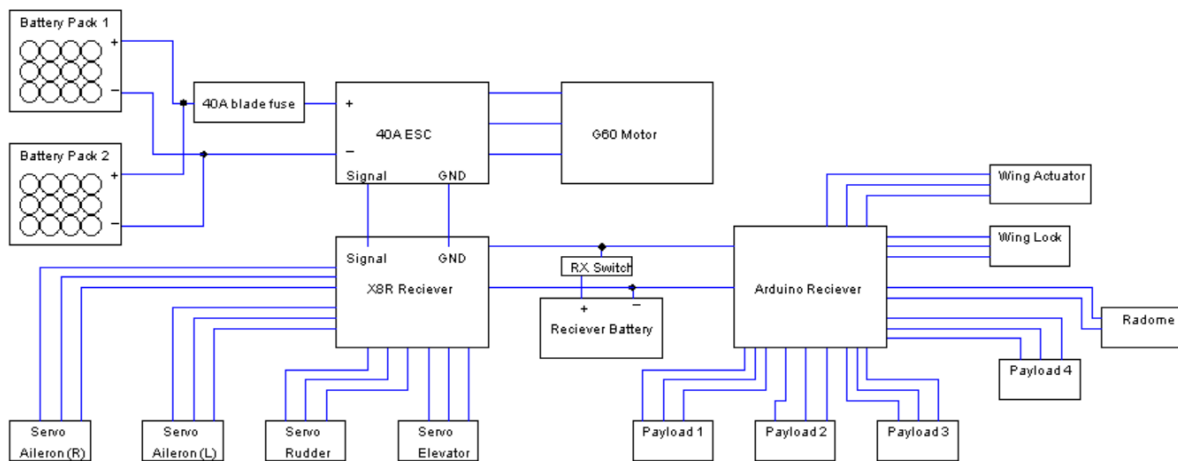


Figure 19: Schematic of all wiring

All of the main systems can be easily analyzed. The radome will be connected only on mission two, otherwise, the terminals will be unconnected.

5.4.2 Payload Mechanisms

The payload mechanism is designed as a claw which mounts to the rib and spar of the wings. The claw mechanism is 3D printed using PLA with high tensile strength, at a low infill since the weight of the payload is relatively small (3 ounces) formed around an individual servo motor. The claw is designed to be modular with a set screw to hold it in place upon the shaft on the wing. This allows the mechanism to

be removed when the plane is put into the stowed configuration. The servo motors are oriented so the center of gravity is located as close to the beam connecting the mechanism to the wing in order to minimize the moment on each mechanism.

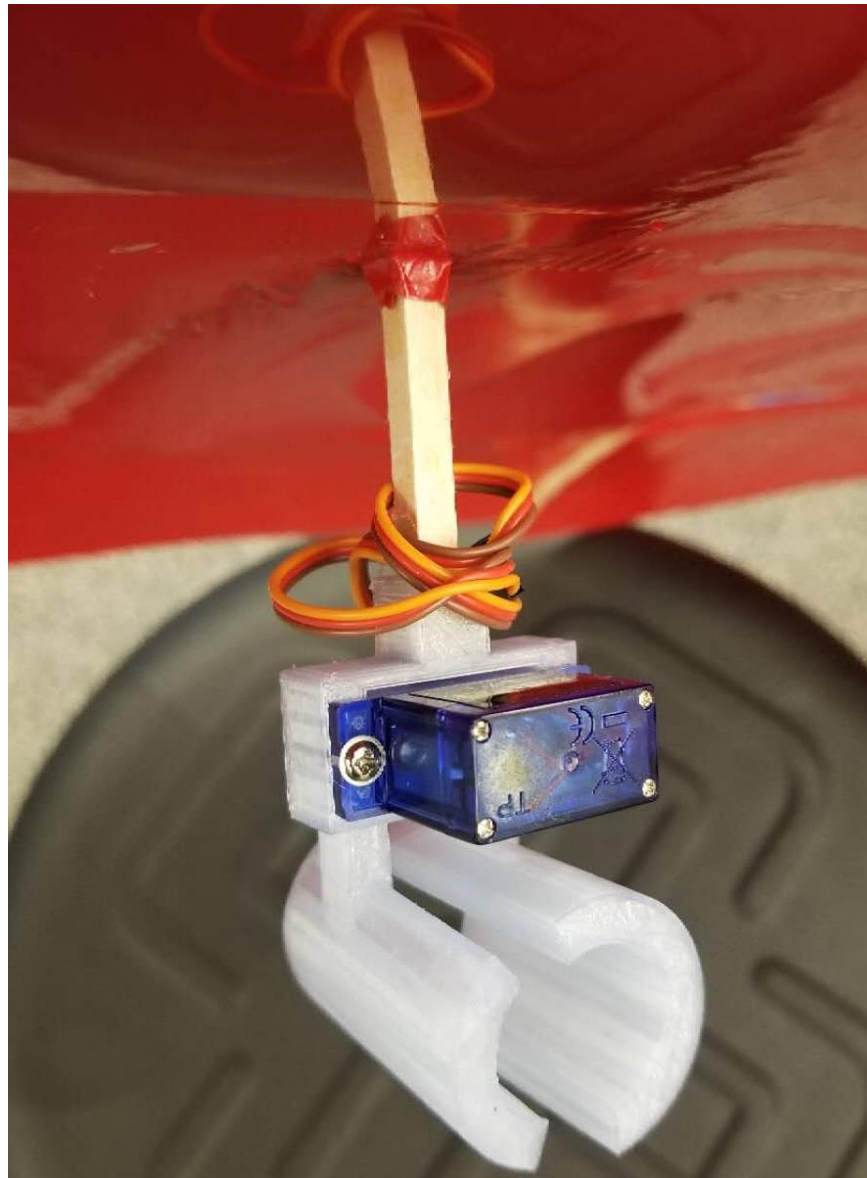


Figure 20: Payload Drop Mechanism

5.4.3 Radome

The radome is designed to be modular and taken off of the plane in order to improve the aerodynamics in the normal flight configuration. The radome is spun by a servo at a low speed from within the radome rather than from the base with a shaft to decrease the stresses on the rotating arm of the servo, allowing a lighter servo to be used. The radome is created from foam in a disc shape then wrapped in monokote wrap to limit the effect on the overall flight characteristics.

The majority of the electronic systems are placed in the fuselage. In particular, the batteries must be located at the calculated center of gravity due to their high mass. The batteries, ESC, servo batteries, RF components, and related wires are secured inside the fuselage via velcro strips and zip ties.

The radome's motor is mounted within a motor housing located at the top of the fuselage. It is programmed to spin 360 degrees around its central axis

The motor and propeller are located at the forefront of the fuselage, at the centerline of the plane. The motor is mounted using screws and Nylocks.

5.4.4 Peripheral RF Actuation

A separate RF system from the Taranis X7 transmitter and the X8R receiver was used to actuate the payload drops, wing movement, wing locking, and radome. An Arduino system using the NRF24 module was used for its flexibility to control many different components. We will use one on the plane to the receiver, and a ground controller with another NRF24 module and Arduino.

The layout of the receiver module and ground actuation controller:

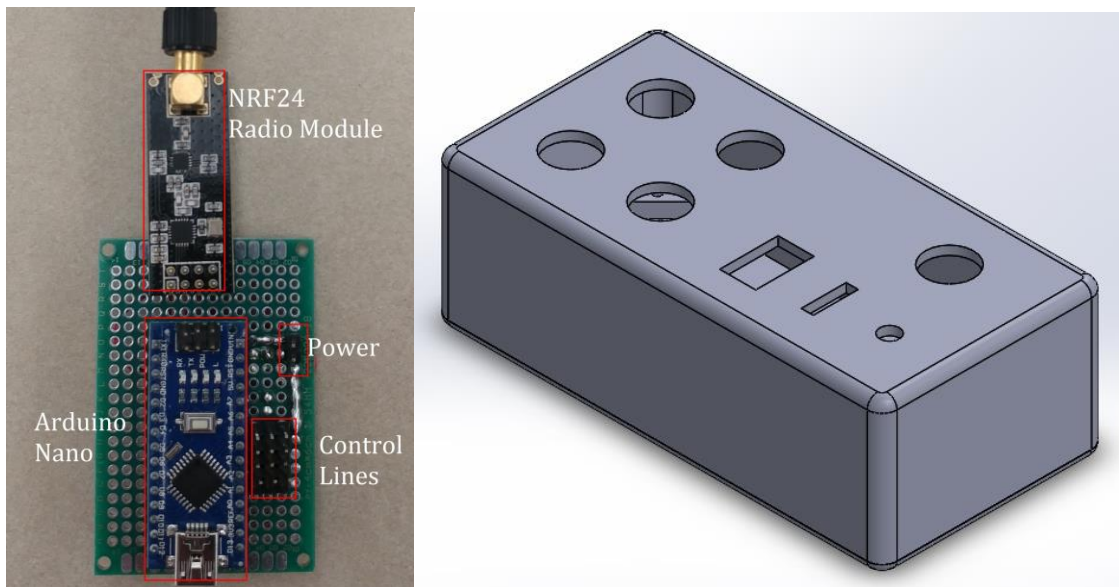


Figure 21: Arduino Transmitter (left) and Mechanism Controller (right)

5.5 Weight and Mass Balance

EW_{plane} for M1, M2, and M3 was 2.017 lb. It is expected that the added weight of glue/epoxy for integration will drive EW_{plane} closer to ~3lb, which is what the team anticipated the weight to be and was already accounted for. The CG location is roughly at ~12 in. , which was kept within the aerodynamic center at ~13.8 in. to maintain the design static margin for all three missions and guarantee a stable flight. In order to accommodate for different weight distributions in different missions that will shift the CG, the flight batteries will be moved forward to compensate for the weight added onto the aircraft. The origin is located at the nose of the aircraft with a coordinate axis as shown in Figure. #. All CG distances shown in Table # are expressed in the airplane coordinate system.

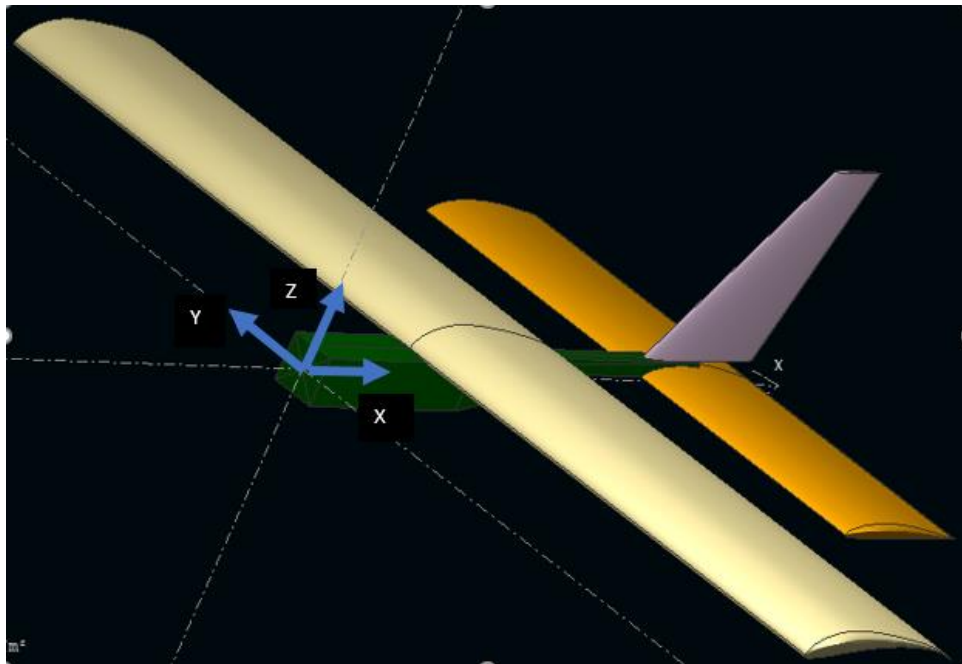


Figure 22: Aircraft Origin Coordinate System.

Table 11: Center of Gravity Analysis

Aircraft Component	Weight	CG Distance from origin in X	CG Distance from origin in Y	CG Distance from origin in Z
	lbs	in.	in.	in.
Fueslage	0.563	12.44	0	0.39
Wing	0.661	12.177	0	2.319
Adapter/BasePlate	0.485	14	0	1.5
Motor/Propellor	0.661	-0.5	0	0
Flight Battery	2.094	8.5	0	-1.5
Speed Controller	0.066	8	0	-1
Reciever	0.033	8	0	-1
Elevator/Rudder Servos	0.242	24	0	1.5
Forward Landing Gear	0.077	0	0	-1.5
Aft Landing Gear	0.088	20	0	1
Radome	0.009	8	0	2
6 Payloads	1.124	12	18	-1

5.6 Flight and Mission Performance

Multiple flight tests were performed on multiple iterations of the design in order to verify the design and adjust for issues. Problems were encountered in the prototypes and solutions were implemented in order to make a working and optimal plane. Subsystems of the plane were tested individually on the ground in order to ensure working components before liftoff. The progress of the iterations can be concisely displayed by the decreasing distances with Alpha requiring 20 ft, Beta requiring 10 ft and Beta 2.0 taking off in 8 ft.

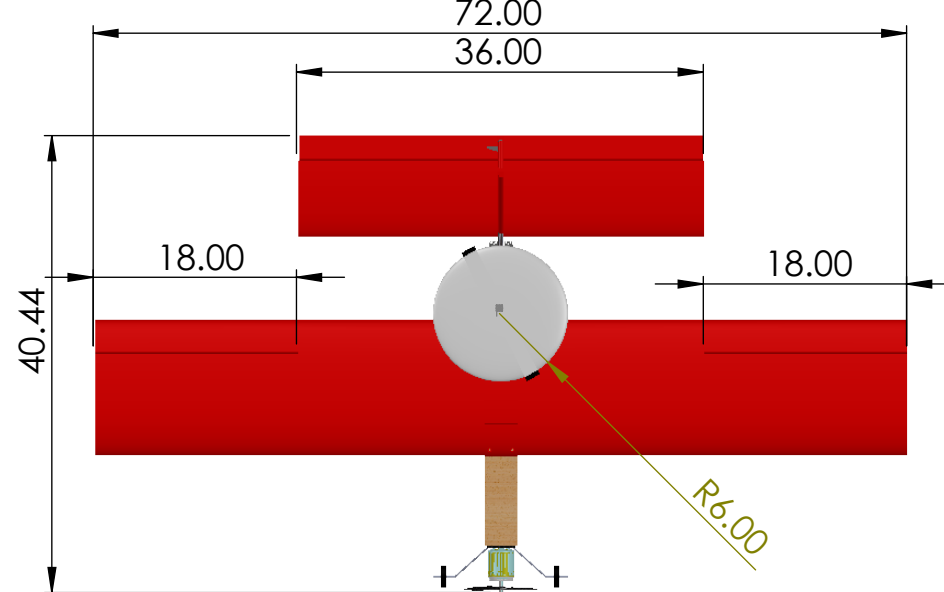
Table 12: Prototype Matrix

Iteration	Flight Objective	Problems	Solutions Implemented in Next Iteration
Alpha	Determine Initial Flight Characteristics	<ul style="list-style-type: none"> -No Payload Attachments -Unstable Controls -No Folding Mechanism -Difficulty Taking off 	<ul style="list-style-type: none"> -Larger Wingspan -Larger Motor -Wooden Fuselage with Boom -Folding Mechanism -Shorter Control Rods

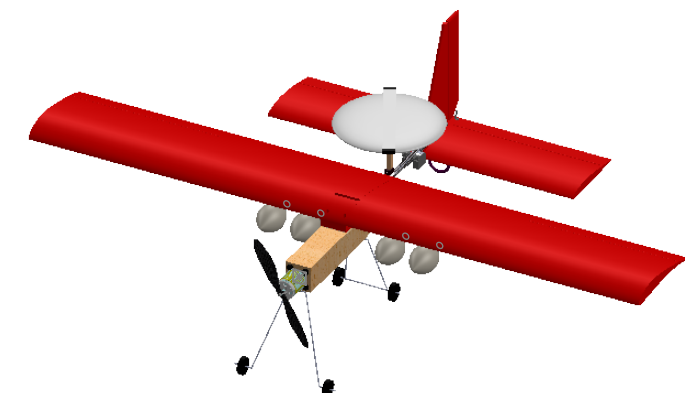
Beta	Determine the Effect of Weight and Material Changes	-Difficulty Taking Off -Unstable Landing Gear	-Larger Angle of Attack -Larger Steel Landing Gear -Larger Propeller
Beta 2.0	Verify Changes & Take Off Distance	Slightly Unstable Controls	-Small Optimizations

1	2	3	4	5	6	
Layout/Bill of materials				Part number	Part	Qty.
				1	17" Propeller	1
				2	G60 500KV Motor	1
				3	Front landing gear	1
				4	Fuselage	1
				5	Back landing gear	1
				6	Attack stores	4
				7	Wing	1
				8	Tail	1
				9	Tail Hook	2
				10	Servo motor	2
				11	Control horn	1
				12	Rudder	1
				13	Radome	1
				14	Folding Mechanism	1
				15	Battery Case	1
				16	Front landing gear	1

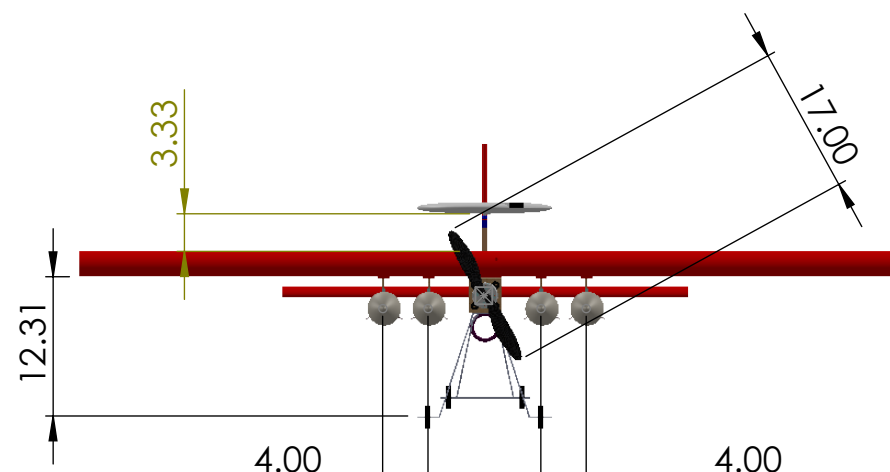
1 2 3 4 5 6



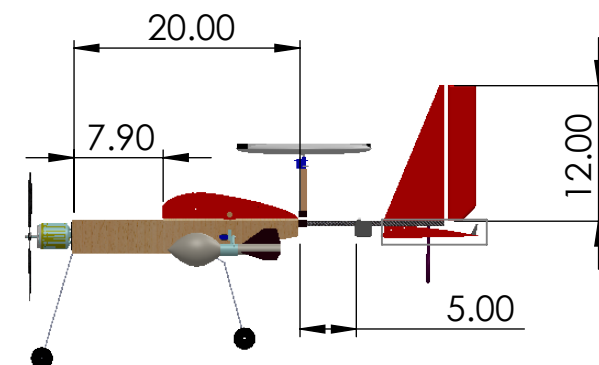
3 View Drawing



ISOMETRIC VIEW



FRONT VIEW



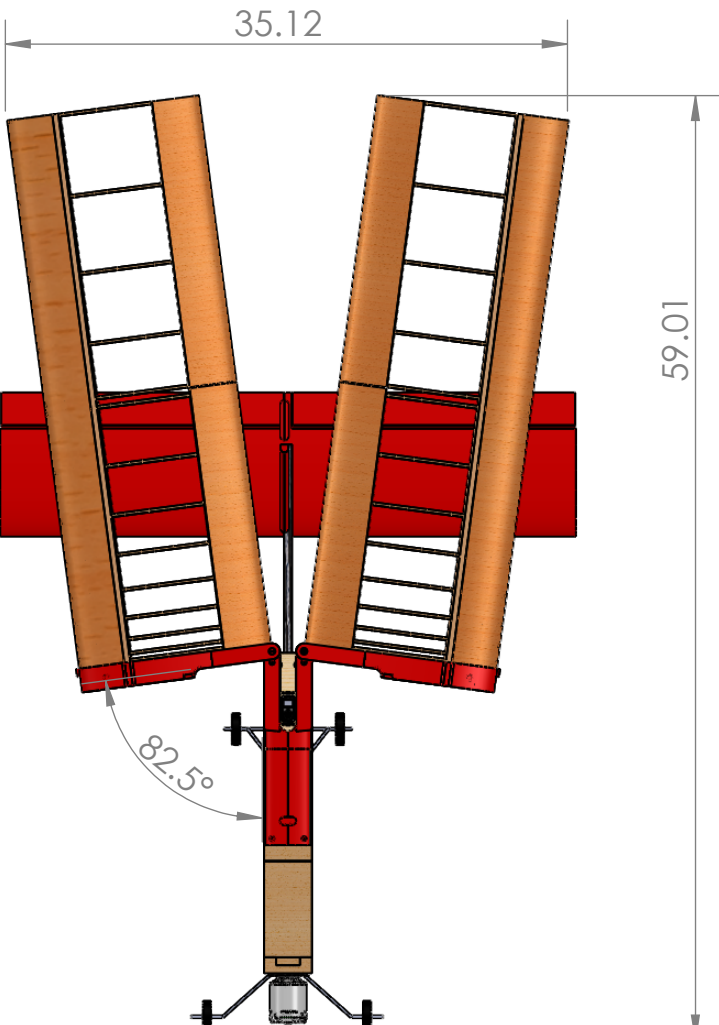
SIDE VIEW

NOTES:

- 1) All dimensions are in inches.

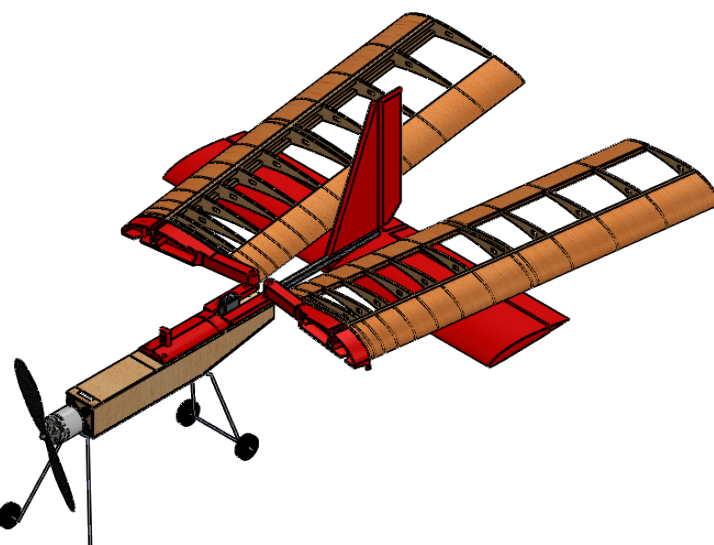
6 5 4 3 2 1

D



Folding Configurations

Stowed Configuration



Flight Configuration



C

B

A

Note: All units are in inches

D

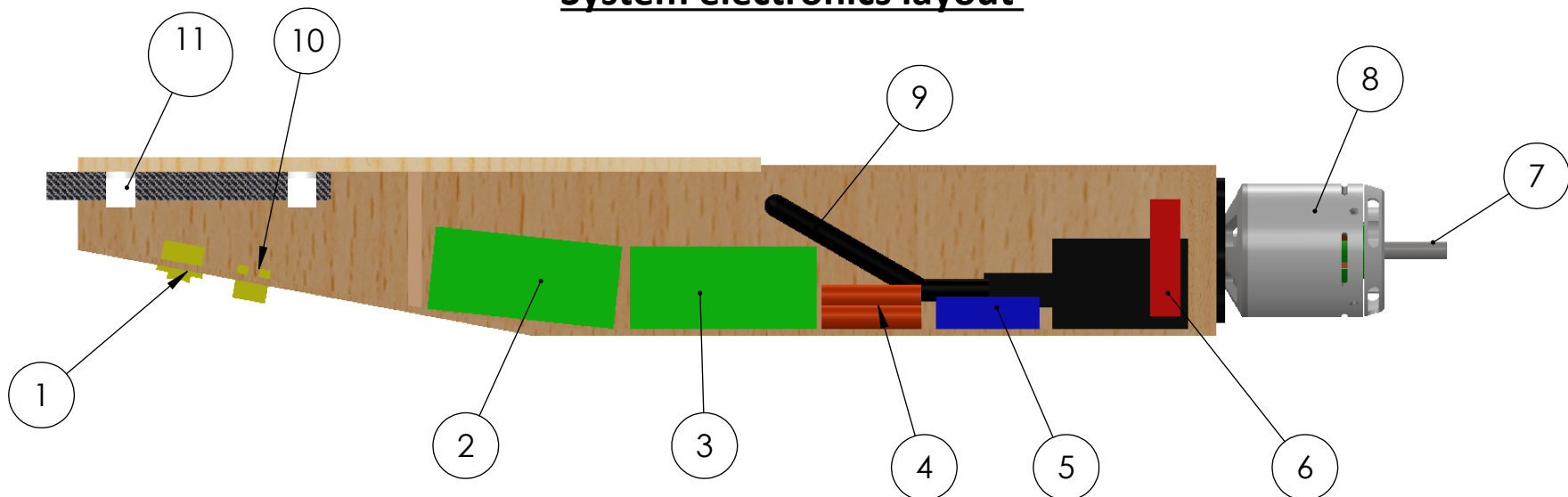
C

B

A

6 5 4 3 2 1

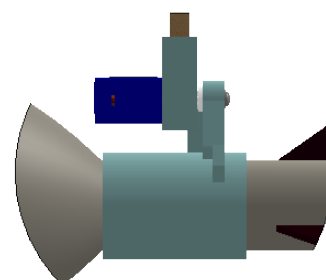
System electronics layout



Sr. no	Part	Qty
1	ON/OFF Switch	1
2	Battery Pack 1	1
3	Battery Pack 2	1
4	Receiver battery	1
5	X8R Receiver	1
6	40A ESC	1
7	Shaft	1
8	500 KV G60 Motor	1
9	Arduino receiver	1
10	40 A amp fuse	1
11	Tail boom attachment	1

6 5 4 3 2 1

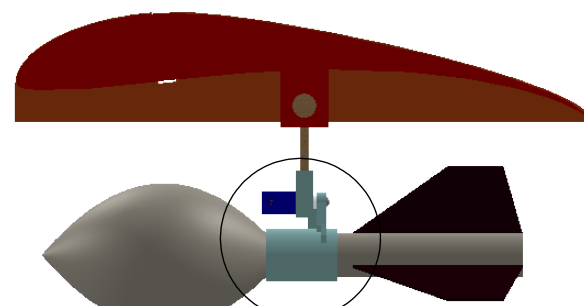
Payload accomodation and drop mechanism



DETAIL A

SCALE 1 : 2

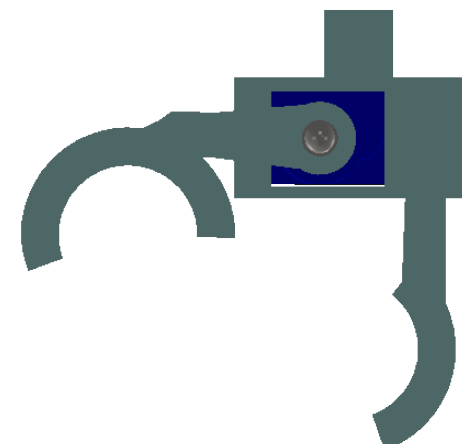
Detailed View



Side View



Closed Configuration



Open Configuration

NOTES:

- 1) The attack store is held from the central stem part.
- 2) Each attack store has a separate servo that can independently open and close the claw mechanism.
- 3) The whole claw structure in light blue color is 3D printed.

A

B

C

D

6.0 Manufacturing Plan

6.1 Manufacturing Methods Considered

Numerous methods were considered for the construction of the aircraft in order to optimize the tradeoff between ease and reparability while also staying within a reasonable weight.

6.1.1 Wing and Control Surfaces

The manufacturing methods of the wings and control surfaces have been selected in order to optimize the tradeoff between weight and strength. The two major considerations for wing design were solid foam wings and ribbed balsa wings.

Solid foam wings are very lightweight, but provide less structure and strength due to the material for the wings and control surfaces. They are known to produce a fluttering effect during flight due to this lack of structure which is undesirable for maintaining consistent and reliable flight characteristics. The foam wings would be manufactured by outlining the shape of the airfoil and cutting the foam with a hot wire. This method of manufacture requires some skill as well as access to a hot wire cutter, though it is a fairly expedient process. It would prove difficult to repair the foam wing if it were to break due to a crash. Solid wings, regardless of the material, present difficulty when running wires or any additional support structures as space for these structures must be cut from the foam, run through it, or affixed to the exterior.

Ribbed balsa wings provide a lightweight and rigid alternative to foam wings. The ribs are manufactured by laser cutting the individual ribs, connecting them with pre-cut spars, and wrapping the structure in thin balsa along the leading and trailing edge then wrapping the entire structure in Monokote heat shrink wrap. Monokote is a light plastic wrap that goes around the structure of the balsa wing, providing a smooth aerodynamic surface. Laser cutting the balsa ribs allows for far greater speed of manufacturing and allows the airfoil to be made to the exact specifications of a CAD file, eliminating human error. Machining the ribs by hand using the scroll saw requires more skill, time, and produces a less exact part. However, laser cutting entails a much higher cost per part than machining by hand using the scroll saw. Constructing the wings using balsa ribs and basswood spars, with optimized structural support, provides a desirable balance between weight and strength and uses the least amount of material possible. Balsa ribbing is also much simpler to repair as individual ribs can be replaced in the event that they are damaged and Monokote is also relatively simple to patch and reseal. A sample of a partially constructed prototype wing can be seen in Figure 23.

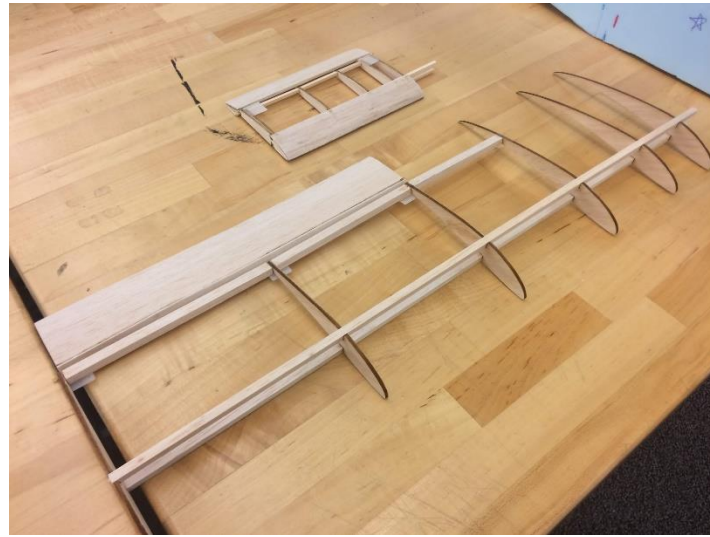


Figure 23: Main wing partially assembled

6.1.2 Fuselage

The structure of the fuselage requires strength and stability in order to protect the electrical components in the event of a crash.

Constructing the fuselage with wood offers greater strength and rigidity at the cost of a larger density. However, using balsa minimizes the increase in weight while maintaining the gains in strength due to its low density and tensile strength in the direction of the wood grain. By placing wood grains perpendicular to each other, balsa's strength can be further optimized in multiple directions. The wooden fuselage is made by gluing together five main panels, several interior bulkheads, a motor mount, and wing mount. Each panel is cut out of a larger sheet using an exacto knife, allowing for selection of the best sections of the wood and best use of the grain. Once assembled and glued in place, the exterior panels of the fuselage is then wrapped in reinforced duct tape to give additional strength and stability in the transverse direction to limit collapse and fracturing of the wood in the event of a crash. The wooden frame also allows for increased rigidity making mounting of structures simpler and more reliable.

6.1.3 Mechanisms

The folding wing and payload release mechanisms must be manufactured for continued, reliable airborne use while maintaining good repairability and a lightweight structure.

The folding mechanism consists of a hinged mount that connects the fuselage to the wings and allows the wings to rotate backward from the back of the wing. The wings are attached through a fishing line to a winch in the center of the fuselage in order to draw the wings into the flight configuration. This design was chosen for its simplicity and lightweight nature in order to increase reparability and ease of manufacture. A wooden prototype of the mechanism can be seen below in Figure 24 where it is seen mounted with prototype wings (without Monokote wrapping) to an early foam fuselage prototype for a proof of concept test.

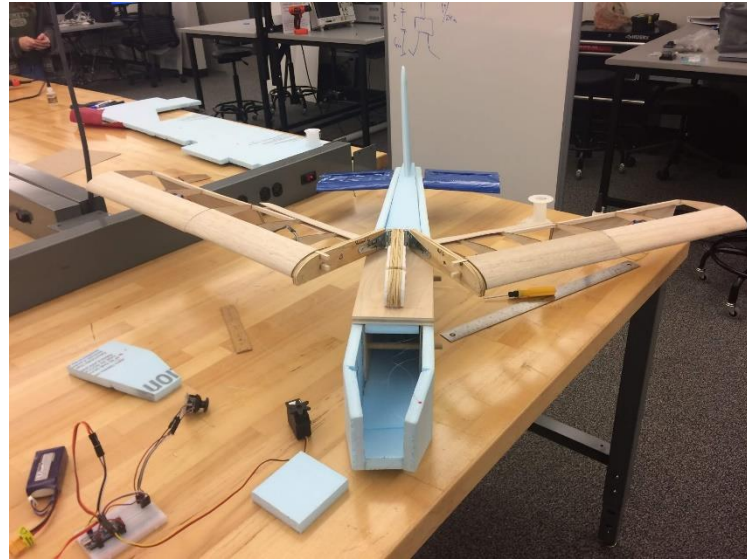


Figure 24: Prototype folding Mechanism

The payload drop mechanisms consist of separate servo motors for each payload claw(see figure 25) that is positioned below the wing ribs along the spars. The separate motors will plug into an arduino which releases each claw independently. The claw itself is a hollow cylindrical shape that closes around the stem of the attack stores.

The radome consists of three circular foam pieces, two thicker pieces with smaller radii attached to a larger radius but thinner foam piece smoothed into a symmetrical disc shape to limit drag. The disc is attached to a wooden mount with epoxy which is then attached to the servo motor with more epoxy. The servo is also attached to the vertical post with epoxy and the post is secured within the fuselage with a bolt and clamp assembly.

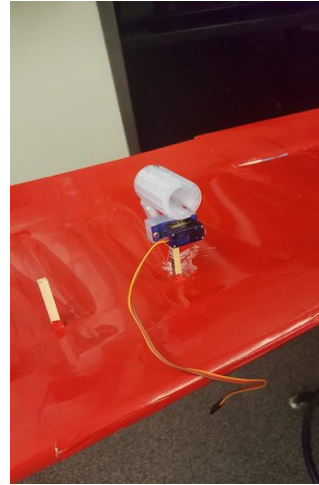


Figure 25: Payload drop mechanism

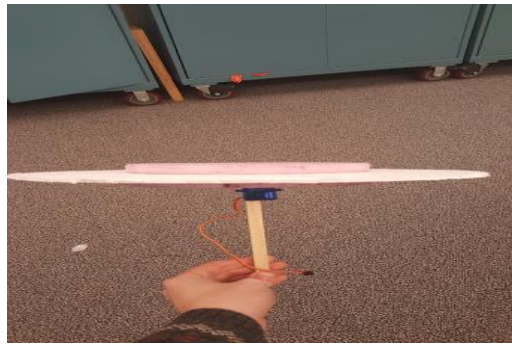


Figure 26: Radome

The hinge, wing mount, and claws are all 3D printed due to the importance of a low tolerance for the points of attachment between the parts and the unique geometry required for the mechanisms.

6.2 Manufacturing Methods Selected

Although many methods of manufacture were considered and prototyped, only a few were implemented on the final design. These methods are chosen for their ease-of-manufacture, repairability and minimal weight addition.

6.2.1 Wing & Tail

The ribbed balsa with Monokote method was selected because it offers a superior strength to weight ratio using easily accessible and affordable materials. Balsa ribs were designed and simulated on in Solidworks, then laser cut by a sponsor from a nearby company. The prototype ribs can be seen below in Figure 27 where both the wing and tail ribs are seen shortly after being laser cut.



Figure 27: Prototype ribs

The ribs have friction fit spar slots and are glued to the spars using CA glue. Strips of balsa less than 0.118 in. wide are soaked in water overnight and formed around the leading and trailing edges of the wing ribs to give a smooth structure of the leading and trailing edge of the wing. The glue is given time to set and then the entire frame is sanded smooth. Ailerons are formed by cutting off a section of the rear portion of the assembled wing (prior to Monokote wrapping), reinforcing the new trailing edge of the wing with spare spars, and then attaching the aileron back to the wing with butterfly style hinges made of woven ribbon.

The Monokote aerodynamic surface is laid taut atop the wing structure then formed around and attached using a heat-sealing iron into position and then shrunk to a smooth fit using a heat gun.

The Vertical Stabilizer is a solid piece of Blue Core Foam sanded into a symmetrical aerodynamic shape using an electric sander at the University of Texas at Dallas Fabrication Shop. The stabilizer is attached to the top of the tail boom with epoxy.

6.2.2 Fuselage

The fuselage panels are cut out of $\frac{1}{8}$ inch balsa sheets, formed around basswood bulkheads, attached together with CA glue, then wrapped with duct tape, to maximize the grain strength and form a very light and sturdy structure.

The tail boom of the plane consists of a hollow square rod of carbon fiber protruding from the rear of the fuselage. The boom is mounted to the fuselage mounting plate using 3D printed brackets, and metal nuts and bolts to allow it to be removed for repair or replacement.

The motor is mounted to a piece of basswood on the nose of the plane using four bolts with nylon lock nuts to limit loosening due to vibration during operation.

The landing gear is mounted to the fuselage by inserting the legs into a 3D printed receiver that is designed to hold the landing gear rigidly in position. The receivers are in turn mounted with epoxy to basswood bulkheads, one in the nose which also serves as the motor mount, and one approximately 15 inches back from the nose of the fuselage. These bulkheads are included to increase the structural strength of the fuselage and prevent it from bowing or deforming under various loads.

6.2.3 Electronics Installation

The servo motors and wires are attached within the wing using CA glue and thread through holes within the ribs and adapter all the way into the fuselage to limit drag and interference with the aerodynamic structures. The servos are connected to the control surfaces using control rods hooked into control horns which are sealed with epoxy onto the control surface. The receiver, electronic speed controller, and batteries are installed inside the fuselage along the centerline to align the center of gravity with the optimal position for the aircraft as found through the XFLR5 software. Due to their significant weight, the batteries are affixed to the interior of the fuselage with velcro pads on the bottom panel. The servo motors that control the elevators and rudder are attached externally to the tail boom on either side with epoxy.

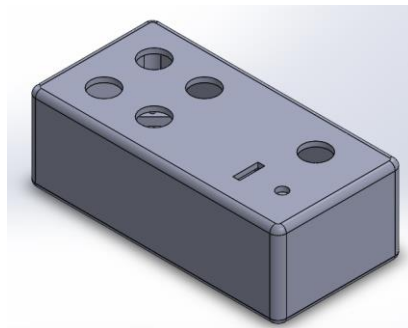


Figure 28: Controller Case

Regarding the payload drop, it requires the capability to release a minimum of 4 separate stores; this issue was resolved with the use of an arduino connected to a separate controller as pictured in figure 28. The top four buttons activate each attack store independently while the bottom two rocker switches control the radome and folding wing lock.

6.2.4 Mechanisms Installation

The attack store release mechanisms are attached to posts extending out of the underside of the wings. These posts are attached with CA glue to a rib and the spars within the wing for stability. The mechanisms are slotted onto the posts and held in place with setscrews to allow for removal when the plane is entered a stowed configuration.

The radome is a Monokote wrapped foam disc affixed to a servo motor atop a wooden post extending from the top of the fuselage. The post is rigidly attached into the fuselage with a clamp apparatus created out of 3D printed brackets with nuts and bolts to vary the clamp position. This allows the radome to be removed for repairs and when the plane is placed into a stowed configuration

The wing folding mechanism is a 3D printed assembly consisting of a central base with a wing adapter on each side attached via hinges in the rear of the mechanism. These adapters are attached to the wing structure themselves by inserting the ends of the spars of the wings into the moving part of the hinge and sealing them with epoxy. The interior side of the innermost rib is made flush with the adapter and also sealed with epoxy. The central base is bolted to a basswood mounting plate atop the fuselage in order to ensure stability during flight and to withstand the force of the lift on the wings. Bolting the mechanism to the fuselage in this manner allows the wing to be removed for simple transport and repair.

6.3 Manufacturing Milestone and Schedule

The Gantt chart below was created during the first half of the 2018 Fall Semester. The chart below shows the timeline of our process that led to building two prototypes.

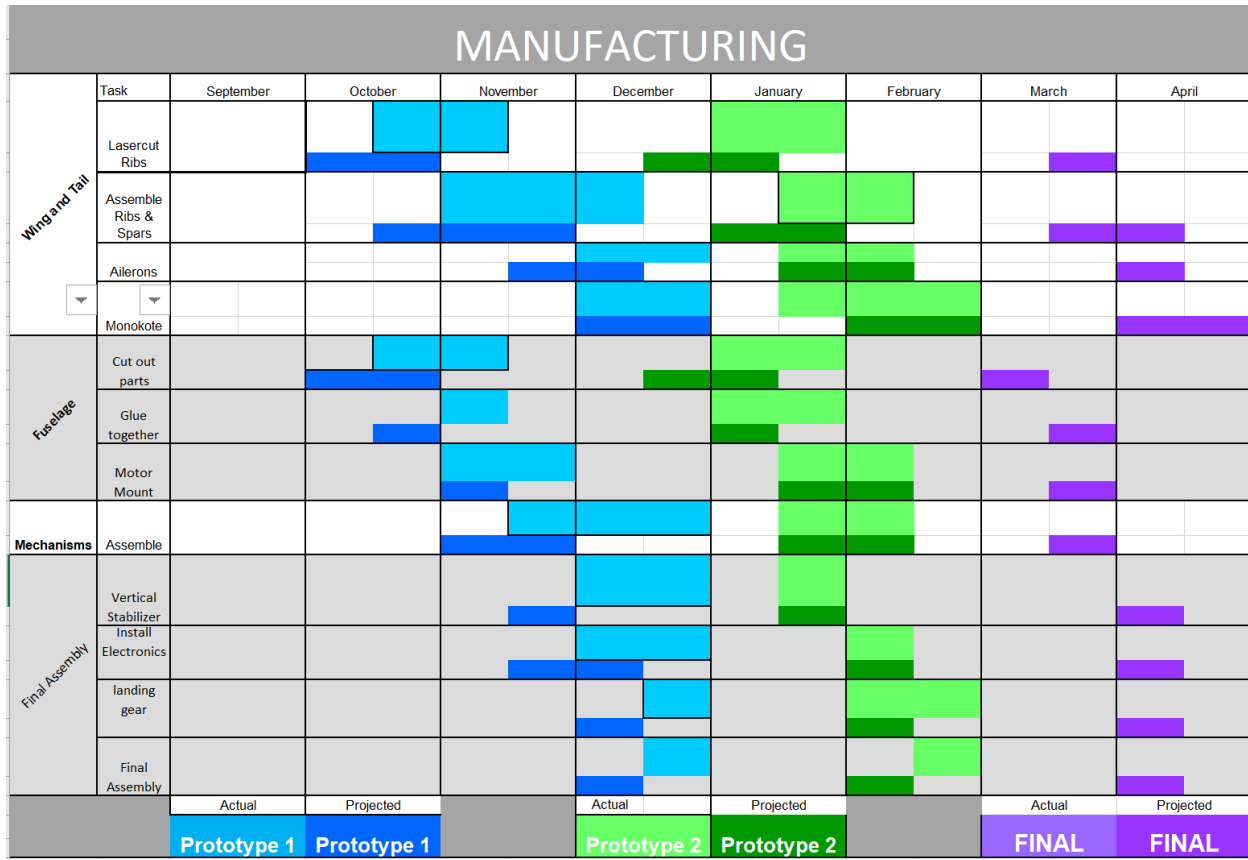


Figure 29: Aircraft Manufacturing Milestone Chart

7.0 Test Planning

A critical analysis of each of the subsystems would ensure that the plane will be optimized for successful flight. If errors are discovered, an iterative process would be used to eliminate potential problems. The overall goal is to achieve the highest score possible, and implementing a schedule that is strictly followed will ensure that we achieve that goal efficiently.

7.1 Test Objectives

The overall goal is to test the effective implementation of different subsystems. Those subsystems can be characterized into Propulsion, RF testing, Aerodynamic Testing, Mechanism Testing. The following documents the cumulative goals for each subsystem.

Propulsion

- Optimize the combination of motors, batteries, and propellers to provide the most thrust as well as the most efficient current draw.
- Confirming simulation data from XFLR5 for takeoff thrust.
- Testing flight duration to confirm battery capacity is sufficient.

RF Testing

- Testing transmitter range through distance tests.
- The overall reliability of data relay and continuous transmission.

Aerodynamic Testing

- Confirm XFLR5 lift projection and take off data.
- Ensure that aerodynamic stability in the aircraft is sufficient for competition.

Mechanism Testing

- Ensure that the folding mechanism will survive wind speed.
- Ensure that the payloads will drop at the desired location.
- Ensure that the radome will spin at the desired paths.

7.2 Subsystem Testing

7.2.1 Propulsion

To determine powertrain efficiency with a different motor, battery, and propeller configurations, a test stand was built. Tests on different transmitter and receiver systems for payload dropping and wing actuation will also need to be conducted for reliability and range tests.

To test the powertrain the test stand was used to measure the voltage, amperage, thrust, and throttle position. By using the test stand, the calculations made on the prop pitch and diameter can be validated. Based on the data from XFLR5, it was determined we needed approximately 2.5kg of thrust for take off. The Turnigy G60 motor was chosen because of its good efficiency compared other motors tested, like the Turnigy D3548/4 motor. The main objective was to test different motors with different propeller sizes and pitches.

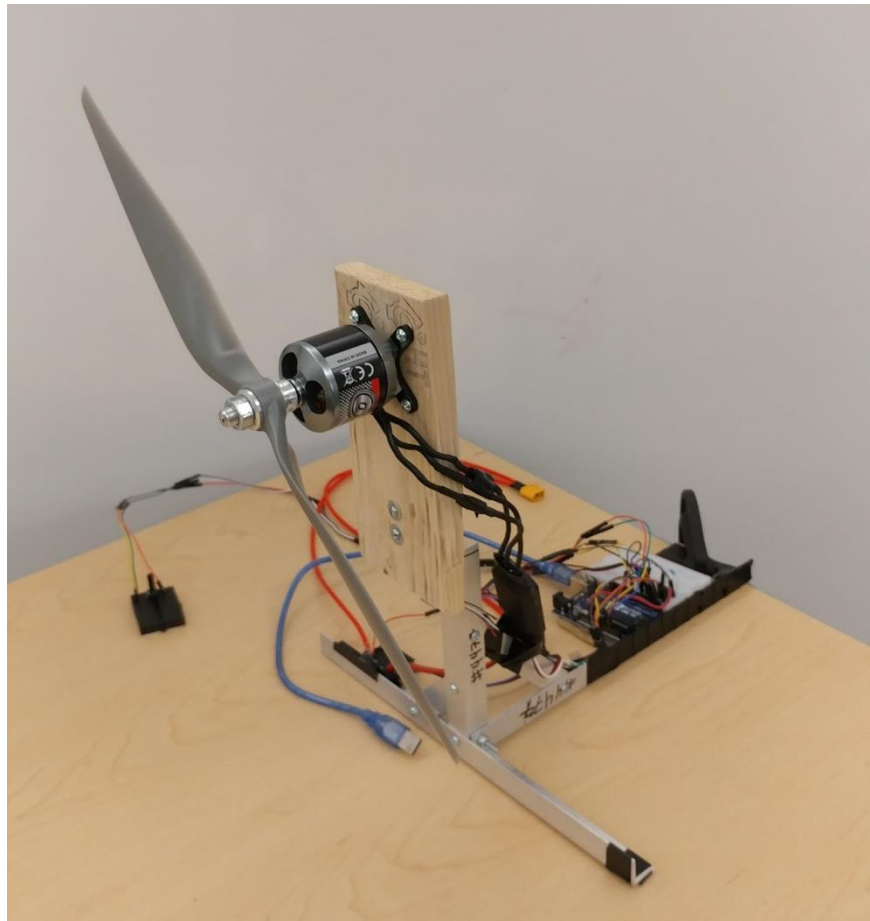


Figure 30: Test stand for Motor and Propeller

7.2.2 RF Testing

For the receiver and transmitter, the Arduino Nano was tested with the NRF24 2.4GHz module for payload, wing actuation, wing locking, and radome. We will test the range of the module and the reliability in close and far range settings.

7.2.3 Aerodynamic Testing

During each flight test, the aerodynamic performance of the aircraft will be closely monitored. It is crucial that the aircraft is capable of generating the calculated lift values during takeoff and clear the launch ramp. During the flight, the aircraft's stability will also be checked to ensure it matched theoretical values. Aircraft stability will be checked by measuring climbing rate, turning rate, and how easily the aircraft is able to pivot on its 3-axis. Control and flight surface flutter will be observed as the airplane flies by and experiences headwind. If too much flutter is observed, the aircraft's control rods will be appropriately stiffened.

7.2.4 Mechanism Testing

During testing, the goal was to determine the best configurations to grab the payloads that are lightweight and effective. A couple different configurations were tested: a few different four-prong claws and an enclosure for the darts. We will also be testing different radome designs to find the lightest design and different ways to attach the radome. These designs will be inspected for their ability to hold up to the forces of flight as well as hold and release the payloads/radome. Also, the folding wing is tested to determine the optimal configuration in terms of ease of repair and simplicity of design. The design for the folding mechanism of the wing does not have to be able to withstand the impact of the movement in the air during activation but it does require an automatic locking mechanism in order to hold the wing secure in flight.

7.3 Flight Test Schedule and Flight Plan

Figure 31 below details the type and timeline of the flight tests performed over the course of the project period. We began with component testing then proceeded onto individual flight tests, shown in Figure 32. These flight tests sequentially tested various critical functions. Each test had a different focus and the data collected was used to incrementally change the overall design of the aircraft. Testing objectives that were not fulfilled during a flight were reattempted in the subsequent flights.

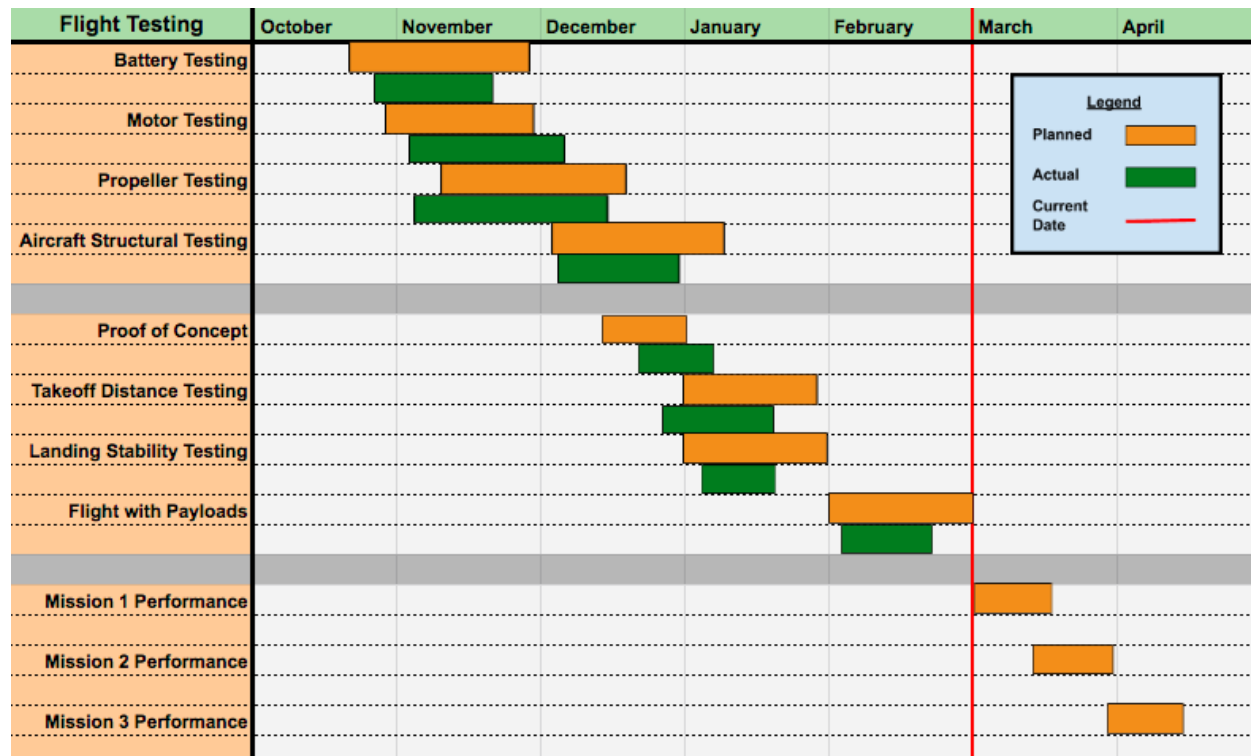


Figure 31: Detailed flight test Gantt Chart

Flight Test	Plane	Wingspan	Focus One	Focus Two	Focus Three
One 1/27/19	“Alpha Enalp”	4 feet	Longitudinal stability	n/a	n/a
Two 2/14/19	“Beta Enalp”	6 feet	Landing gear stability	Propeller size	n/a
Three 2/19/19	“Beta Enalp”	6 feet	New landing gear configuration	New propeller size	Overall Stability

Figure 32: Individual Flight Test Schedule

7.4 Flight Checklist

7.4.1 Pre-Flight Checklist

The following table shows the teams pre-flight checklist. The list starts with the body of the plane where the team does a balance check, monokote, and landing gear check. Following the body, the team will check the wings to make sure they are flight ready. Finally, after the physical body is checked the team will read go through a systems check. This checklist was meant to be filled out make sure there is flight and to ensure the team's safety.

Component	Check	Inspection Task
Body		Pitch Balance - Balances on two pre-determined points marked on the wings Roll Balance - Does not roll when suspended by two strings Check for monocoat cracks Propeller motor secure Propeller spins freely Landing gear firmly attached Wheels spin freely
Wings		Wing-tip test Wires secured Attack store clamps neither stuck nor loose Ailerons and rudder move freely Ailerons and rudder servos securely connected to their flight surfaces
Systems Tests		Check battery voltage Controller connected to receiver on plane All elements respond to controller Check fail-safe switch Check polarity of ailerons and rudder for turning Right turn: Starboard aileron up, port aileron down, rudder points to starboard Left turn: Starboard aileron down, port aileron up, rudder points to port

Figure 33: Pre-flight Checklist

Mission Number	Check	Inspection Task
Mission 2		Radome servo and wires secure
		Radome rotates with remote activation
Mission 3		Attack store clamps remotely open and close
		Attack stores remain secure with agitation of aircraft

Figure 34: Mission specific pre-flight checklist

Notes: *Pitch Balance* - Along the line of the CG and approximately two inches from the fuselage

Roll Balance - Using two strings, one around the propellor motor and one around the fuselage in front of the tail

The Pre-flight checklist is designed to keep the team members safe as well as ensure a quality test every time. The checklist requires team members to do a thorough quality inspection and possible necessary repairs before flying the aircraft. This allows the team to assume that no extraneous factors impacted each test and can analyze the data accordingly.

7.4.2 Post-Flight Checklist

Table 13

Post-flight	Check	Inspection Task
Physical Inspection		Re-inspect monocoat for damage
		Remove batteries and place them in charging station
		Replace batteries
		Check that landing gear is secure

The Post-Flight checklist serves to ensure the safety of the team members when working with powerful motors with large props as well as prepare for the next test. It does this by requiring the removal of the batteries and inspecting the damages caused in the test, also allowing the team to examine points of failure.

8.0 Performance Results

8.1 Demonstrated Results of Each Sub-system

8.1.1 Propulsion Test

The results of the propulsion tests helped confirm motor specifications, while concurrently confirming propeller and battery choices. For the Turnigy G60 motor, our chosen motor, we tested multiple propeller designs to find the maximum thrust needed for takeoff. The three propellers tested were: 15x8, 16x8, and 17x7. After these three trials, the 17x7 propeller was found the best fit for the requirements of power and thrust.

During the max thrust phase, the following power formula was used: Power = Current * Voltage

Table 14

Prop Size	Current	Voltage	Power	Max Thrust
15x8	30 A	12.3 V	369.0 W	2.1 kg
16x8	34.3 A	11.8 V	405.9 W	2.4 kg
17x7	36.4 A	11.5 V	418.6 W	2.6 kg

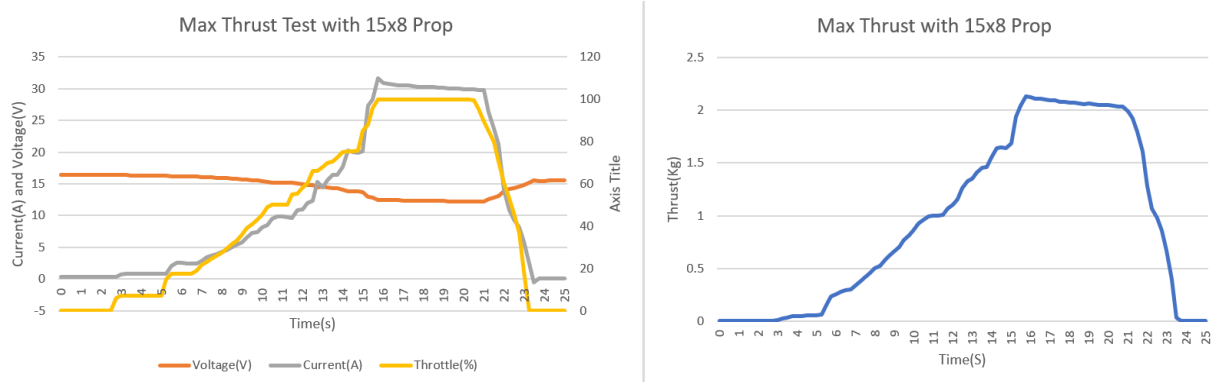


Figure 8.1.1.2 - Test results for the 15x8 propeller using 12s2p NiMh battery packs and G60 motor

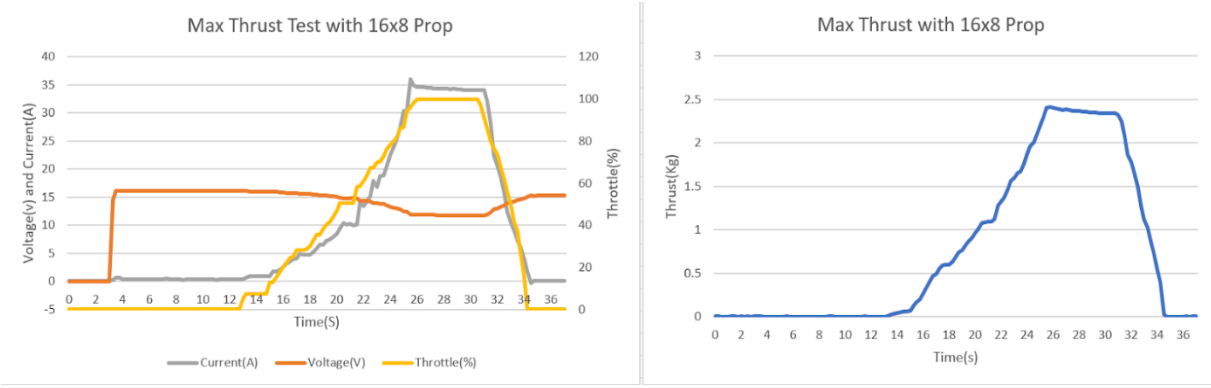


Figure 8.1.1.3 - Test results for the 16x8 propeller with the same battery and motor

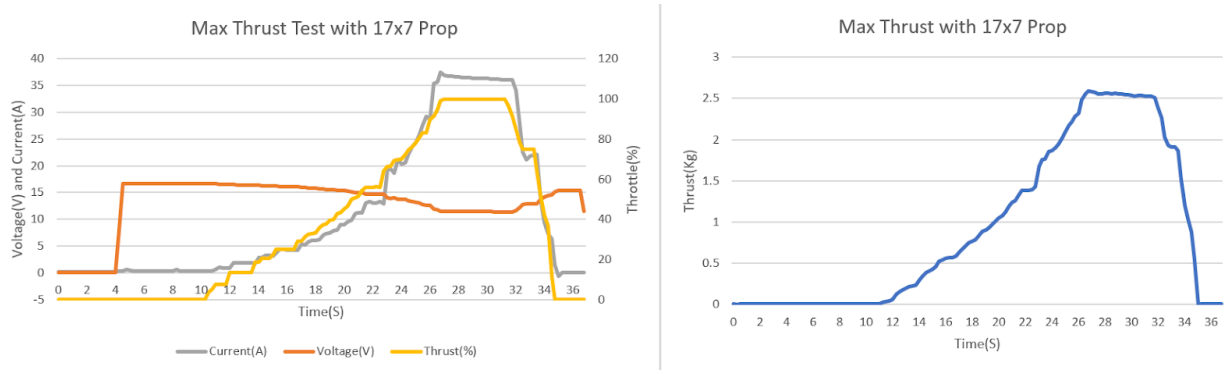


Figure 8.1.1.4 - Test results for the 17x7 propeller with the same battery and motor

In order to take off within the 10-foot ramp specification, the highest thrust propeller and motor combination were needed. The 17x7 propeller was the optimal choice because it did not draw significantly more power than the other propellers while producing the highest thrust.

After deciding to use the 17x7 propeller, a battery drain test was conducted with the test stand to validate the batteries and motor. To test the final powertrain setup the throttle was set to 70% which would produce a slightly higher thrust than required at cruising speed.

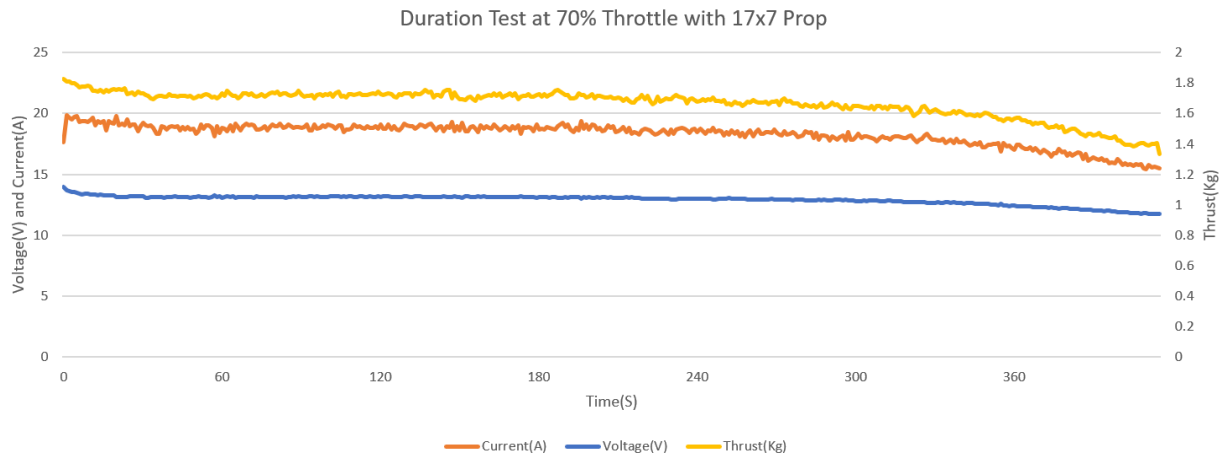


Figure 8.1.1.5 - 17x7 Prop Duration Test

Based on this data, we would be able to run continuously at 70% for approximately 7 minutes. We calculated the time for 1 lap to be approximately 1 minute, this allows us a buffer to drop our 4 payloads with enough time to continue flying if needed.

8.1.2 RF Test Results

To test the Arduino Transmitter and receiver system we set the antennas both perpendicular to the ground and walked out to different lengths to ensure it is still a receiver. We walked to a distance of 500m with the line of sight. The system successfully relayed the data up to 500m. The test distance will be further than any point on the course, leaving plenty of room for margin. This ensures the Arduino RF system will be reliable during the competition.

8.1.3 Aerodynamic Test Results

The testings that were conducted confirmed the theoretical values calculated for lift, aerodynamic stability, and structural stability. The aircraft was able to take off within the 10 ft launch ramp and continue to stay airborne throughout the duration of all testings. Furthermore, the aircraft was described by the pilot to be easy to control and maneuver with. Battery measurements taken after each test flight confirmed expected drag values and anticipated maximum flight times. The aircraft experienced moderate levels of flutter on its first flight but that issue was quickly resolved. Further testings produced little to no flutter.

8.1.4 Mechanism Test Results

Mechanism Testing included the static testing of the claw with payload releasing it. Testing exposed the need for the claw to be able to grasp many sizes of dart since the exact dimensions were not given. Similarly, the radome was tested in a static environment by allowing it to spin freely on the ground.

The folding wing mechanism was also tested on the ground, as a final test since that is the final operating condition. It was tested in the prototyping stage with wooden and metal components and then refined and designed to be 3D printed and tested in that configuration. The radome was then tested in motion, verifying the necessity for the servo to be placed as near the motion of the radome as possible. Additionally, the payload claw drop mechanism was verified in a dynamic environment after a redesign and static testing.

8.1.5 Failsafe

The failsafe for the plane will be programmed directly into the Taranis Q X7 through the settings on the transmitter. After setting these fail-safes the plane will do all the following when there is an RF break: throttle closed, full up elevator, full right rudder, full right aileron, and full flaps down

8.2 Demonstrated Flight Performance of Completed Plane

A few test flights were carried out to validate predictions of aircraft performance. The goal of the flight tests was to evaluate the performance and capabilities of the detail design aircraft. Table 8.2.1 summarizes the flights to date as well as future flight test plans.

Date	Description	Problems	Solutions
27-Jan-19	Determine preliminary sizing	Not enough lift generated	Implement a larger wingspan
14-Feb-19	Propulsion Sizing	Roll stability	Adjusted aileron trim
19-Feb-19	Propulsion Sizing, Stability	Yaw stability	Adjusted landing gear and rudder trim
1-Mar-19	Stability	N/A	N/A
10-Mar-19	Maximum attack stores	N/A	N/A

Table 8.2.1 - Flight Performance and Objectives

As shown, from the flight test data, the first test resulted in not enough lift generated, which meant that an increase in wingspan is necessary to complete the designated missions. In the second flight test, after increasing the wingspan, the plane took off properly, however, did not maintain a stable roll, therefore,

adjustments to the ailerons were made to correct for roll stability. In the third flight test, the aircraft was able to take off maintain a stable pitch, though, it was discovered that the aircraft tends to lean right when rolling on the ground, therefore adjustments were made to the landing gear and to the rudder control horns to adjust for the yaw stability. In future flight tests, the plan is to maximize the number of attack stores while maintaining stability and remain within boundaries of mission requirements. Overall, the team successfully completed three different flight tests and comparing the predicted and actual data are compared in Table 8.8.2.

	Parameter	Predicted	Flown	Percent Error
M1	Flight Speed	8.6 ft/s	8.5 m/s	N/A
	Cruise Current	7.8 A	N/A	N/A
M2	Flight Speed	8.7 ft/s	9 ft/s	11%
	Cruise Current	8.0 A	8.2 A	24%
M3	Flight Speed	8.8 ft/s	9.1 ft/s	32%
	Cruise Current	7.9 A	8.0 A	12%

Table 8.2.2 - Mission speeds, predicted vs. actual

As shown in the table above, predicted flight speeds are ~ -20% lower on average and cruise currents were found to be higher than predicted. The difference between the actual and predicted was deemed to be because of the ambient air conditions at time of flight test, additionally, predicted data was collected based on ideal ambient conditions. These results were used to improve upon the performance of the aircraft and the team plans on reducing error as much as possible by accommodating for ambient conditions predicted on competition day. The following figure shows Enalp in the air on one of the successful flights.



Figure 8.8.3 - A successful flight test on February 13th at Dallas, Texas

Bibliography

- [1] Boeing, “Boeing V-22 Osprey”, *Boeing*, <https://www.boeing.com/defense/v-22-osprey/> [retrieved 20 December 2018]
- [2] UIUC Applied Aerodynamics Group, “UIUC Airfoil Coordinates Database” *University of Illinois-Urbana-Champaign Airfoil Database*[Online Database], 2018, https://m-selig.ae.illinois.edu/ads/coord_database.html
- [3] HobbyKing, <https://hobbyking.com/> [retrieved 15 January 2018]
- [4] MatWeb LLC, “Search Results”, *Material Property Data*, 1996-2019, <http://www.matweb.com/search>
- [5] The Dow Chemical Company, “STYROFOAM™ Panel Core 30 Extruded Polystyrene Foam Insulation” <http://msdssearch.dow.com/PublishedLiteratureDOWCOM> [retrieved 12 December 2018]
- [6] “Super glue® Safety data sheet”, *National Centre for Biotechnology Education*[online], 26 June 2015, <http://www.ncbe.reading.ac.uk/SAFETY/SDS/Superglue.pdf>
- [7] Daniel P. Raymer “A Conceptual Approach,” *Aircraft Design*, Sixth Edition,30 September 2018
- [8] An Introduction to SOLIDWORKS Flow Simulation, 2018.
- [9] Stability analysis using XFLR5, A. Deperrois - November 2010.